The plant cell wall integrity maintenance and immune signaling systems cooperate to control stress responses in *Arabidopsis thaliana*

Timo Engelsdorf[1, ⌘], Nora Gigli-Bisceglia[1], Manikandan Veerabagu[1, £], Joseph F. McKenna[2, ×], Lauri Vaahtera[1], Frauke Augstein[1, †], Dieuwertje Van der Does[3, ≈], Cyril Zipfel[3] and Thorsten Hamann[1, *]

[1] Department of Biology, Høgskoleringen 5, Realfagbygget, Norwegian University of Science and Technology, 7491 Trondheim, Norway.

[2] Dept. of Biology, Imperial College London, South Kensington Campus, SW7 2AZ London, UK

[3] The Sainsbury Laboratory, Norwich Research Park, Norwich, NR4 7UH, UK.

⌘ Present address: Department of Biology, Division of Plant Physiology, Philipps University of Marburg, 35043 Marburg, Germany

£ Present address: Department of Plant Sciences, Norwegian University of Life Sciences, N-1432 Ås, Norway

× Present address: Plant Cell Biology, Dept. Biological and Medical Sciences, Oxford Brookes University, Oxford, OX3 0BP.

† Present address: Department of Organismal Biology, Physiological Botany, Evolutionary Biology Centre and Linnean Centre for Plant Biology, Uppsala University, Ullsv. 24E, SE-75651 Uppsala, Sweden

≈ Present address: 2Blades Foundation/BecA-ILRI Hub, P.O Box 30709, Nairobi 00100, Kenya

* Corresponding author. Email: Thorsten.hamann@ntnu.no

Abstract

Cell walls surround all plant cells, and their composition and structure are modified in a tightly-controlled, adaptive manner to meet sometimes opposing functional requirements during growth and development. The plant cell wall integrity (CWI) maintenance mechanism controls these functional modifications as well as responses to cell wall damage (CWD). We investigated how the CWI system mediates responses to CWD in *Arabidopsis thaliana*. CWD induced by cell wall–degrading enzymes or an inhibitor of cellulose biosynthesis elicited similar, turgor-sensitive stress responses. Phenotypic clustering with 27 genotypes identified a core group of receptor-like kinases (RLKs) and ion channels required for activation of CWD responses. A genetic analysis showed that the RLK FEI2 and the plasma membrane–localized mechanosensitive Ca^{2+} channel MCA1 functioned downstream of the RLK THE1 in CWD perception. In contrast, pattern-triggered immunity (PTI) signaling components, including the receptors for plant elicitor peptides (*At*Peps) PEPR1 and PEPR2, repressed responses to CWD. CWD induced the expression of *PROPEP1* and *PROPEP3*, which encode the precursors of *At*Pep1 and *At*Pep3, and the release of PROPEP3 into the growth medium. Application of *At*Pep1 and *At*Pep3 repressed CWD-induced phytohormone accumulation in a concentration-dependent manner. These results suggest that *At*Pep-mediated signaling suppresses CWD-induced defense responses controlled by the CWI mechanism. This suppression was alleviated when PTI signaling downstream of PEPR1 and PEPR2 was

impaired. Defense responses controlled by the CWI maintenance mechanism might thus compensate to some extent for loss of PTI signaling elements.

Introduction

Plants adapt to diverse environments by modifying their architecture. The cell walls surrounding all plant cells are key elements enabling this adaptability and consist of different components including proteins and polysaccharides such as cellulose, hemicelluloses, pectins, and lignin (1). These components are synthesized in different subcellular compartments and have specialized functions. Cellulose is synthesized by plasmamembrane-localized cellulose synthase complexes and released into the adjacent extracellular space as strands that form microfibrils before being incorporated into the wall where they function as the main load-bearing element. The walls are also essential elements underlying growth, development, and resistance to biotic and abiotic stresses, all of which influence crop yield (2, 3). This is illustrated by mutations that improve yields of staple crops like maize and rice by affecting cell wall biosynthesis, homeostasis, polysaccharide modifications, and signaling components (4, 5).

Cell wall plasticity describes the ability of plant cell walls to adapt to dynamic and challenging growth conditions. Plasticity and the resulting recalcitrance in cell wall biochemistry and structure against targeted manipulation also represent a major challenge to producing energy from lignocellulosic biomass (6). The available evidence suggests that the plant cell wall integrity (CWI) maintenance system forms an integral element of cell wall plasticity (7–9). This mechanism seems to involve receptor-like kinases (RLKs) and ion channels that constantly monitor the state of the cell wall and initiate adaptive changes in both cellular and cell wall metabolism in response to cell wall damage (CWD) (10–12). Here we refer to any changes to cell wall structure or composition that impair CWI as CWD. Because

CWD may be induced by various means, both ligand-mediated mechanisms and mechanoperception could be involved in CWD detection. For example, pathogen-derived enzymes break down cell walls, which releases cell wall–derived fragments. This could lead to cell wall weakening, deformation, displacement of the cell wall relative to the plasma membrane and can eventually result in cell bursting due to the high turgor pressure of the cell (13, 14). The cell wall fragments, such as cellobiose or oligogalacturonides (OGs, fragments of pectic polysaccharides), can activate plant immune responses (15, 16). Whereas OGs are detected through wall-associated receptor kinases (WAKs), the receptors for cellobiose have not been identified (7). Mechanosensitive systems may also be activated by CWD that compromises the structural integrity of the cell wall (17). In addition to the enzymatic actions of pathogens and mechanical damage caused by breakage or grazing, defects in cell wall biosynthetic processes can also cause CWD by preventing the production of load-bearing structural elements (18).

Although several candidate genes have been implicated in CWD perception, experimental evidence confirming their involvement is scarce (7, 10, 19). Amongst the candidates identified in *Arabidopsis thaliana* are two homologs of plasma membrane–localized RLK1-like proteins originally in *Catharanthus roseus* (CrRLK1Ls): THESEUS1 (THE1) and FERONIA (FER) (20, 21). Additionally the leucine-rich repeat (LRR) RLK MALE DISCOVERER 1 (MDIS1)-INTERACTING RECEPTOR-LIKE KINASE 2 (MIK2), WALL-ASSOCIATED KINASE 1 (WAK1) and WAK2, as well as the putatively stretch-activated, mechanosensitive Ca^{2+} channel MATING PHEROMONE INDUCED DEATH 1 (MID1)-COMPLEMENTING ACTIVITY 1 (MCA1) have also been implicated in CWI maintenance in Arabidopsis (22–26). MCA1 was

originally identified through its ability to partially complement a *Saccharomyces cerevisiae* strain deficient for *MID1-CCH1 (Mating pheromone–induced death1–calcium channel homolog1)*, which is required for CWI maintenance in this yeast (22, 27). Homologs of MCA1 and THE1 have been identified in *Oryza sativa* (OsMCA1), *Zea mays* (NOD) and *Marchantia polymorpha* (MpTHE), suggesting that these proteins may participate in cell wall maintenance across the plant kingdom (28–30). A characteristic feature of THE1, FER, WAK1, and WAK2 is the presence of domains that may bind cell wall–derived epitopes or ligands (8, 10, 31). However, binding to cell wall components has been confirmed only for WAK1, WAK2, and FER (8, 21, 32). THE1, FER and MIK2 are required for resistance to the fungal pathogen *Fusarium oxysporum* f. sp. *conglutinans*, implicating CWI signaling also in biotic stress responses (25, 33).

CWD induced by the inhibition of cellulose production stimulates the compensatory production of the cell wall components callose and lignin, accumulation of the hormones jasmonic acid (JA), salicylic acid (SA) and ethylene, generation of reactive oxygen species (ROS), and activation of Ca^{2+}-based signaling, implicating all of these processes in CWI maintenance (11, 23, 34–37). CWD in *Arabidopsis thaliana* promotes the generation of ROS in the apoplast - the space adjacent to the plasma membrane that contains the cell wall - by RESPIRATORY BURST OXIDASE HOMOLOGUE D (RBOHD) (23). The activity of RBOHD is regulated by both Ca^{2+}-dependent and Ca^{2+}-independent mechanisms, with the latter requiring BOTRYTIS-INDUCED KINASE 1 (BIK1), which is a substrate of BRASSINOSTEROID INSENSITIVE 1 (BRI1)-ASSOCIATED KINASE 1 (BAK1) and other RLKs during pattern-triggered immunity (PTI) (38, 39). BAK1 acts as a co-receptor for LRR-RLKs, and as such

plays an important role in responses to pathogen-associated molecular patterns (PAMPs) such as flagellin, the flagellin-derived epitope flg22, elongation factor-thermo unstable (EF-Tu), and the EF-Tu-derived epitope elf18, as well as damage-associated molecular patterns (DAMPs) such as the *At*Pep1 and *At*Pep3 peptides (40–42). *At*Pep1 and *At*Pep3 precursor peptides are encoded by the *PROPEP1* and *PROPEP3* genes, which are induced by pathogen infection and wounding (43). The precursor peptides are reportedly released into the apoplastic space where they are likely processed to give rise to the active form (43). Application of *At*Pep peptides enhances both expression of their own *PROPEP* genes, creating a positive feedback loop, and PTI-controlled defense responses. PTI and CWI maintenance may complement each other during plant defense, but such regulatory interactions between CWI and PTI signaling have not been characterized (44–46).

Here we investigated the responses to different types of CWD to understand the cellular events underlying CWD perception. We analyzed CWD responses in 27 *Arabidopsis thaliana* genotypes to establish the functions of candidate genes in CWI maintenance and performed genetic analyses to assess whether key CWI signaling elements belong to one or more signaling cascades. We found that CWD induced the expression of *AtPROPEP1* and *AtPROPEP3* as well as the release of a PROPEP3 fusion protein. In contrast, application of *At*Pep1 and *At*Pep3 repressed CWD-induced phytohormone production, thus identifying a mechanism through which PTI signaling and the CWI maintenance mechanism cooperate to regulate defense responses.

Results

CWD responses induced by different stimuli are osmosensitive

We used an *Arabidopsis* seedling–based model system to investigate how plants respond to different types of CWD and elucidate further the role of turgor pressure in CWD perception (11). CWD was induced using either Driselase, a mix of several cell wall–degrading enzymes from *Basidomycetes sp.*, or isoxaben (ISX), a herbicide that blocks cellulose biosynthesis (13, 18). We chose Driselase because this enzyme mix is similar to the enzyme cocktail released by fungal pathogens during infection (47–49). Furthermore, the enzymes lead to cell wall fragmentation, thus directly causing CWD regardless of cell type, differentiation stage, or turgor pressure. We chose ISX because it inhibits cellulose production only in actively elongating cells (for example, in the root elongation zone). It causes CWD in conjunction with the naturally high turgor pressure of plant cells because it reduces the number of load-bearing cellulose microfibrills in the walls, thus making the cell wall susceptible to failure. This is illustrated by the suppression of ISX-induced lignin, callose, JA, SA accumulation, tissue lesion formation, and redistribution of carbohydrates by addition of osmotica like sorbitol or mannitol (11, 50). Similar effects have been also reported in yeast cells exposed to CWD, indicating the importance of turgor pressure in CWI maintenance (51).

First we investigated the effect of ISX or Driselase treatment on the morphology of Wave 131Y seedlings, which ubiquitously express membrane-localized yellow fluorescent protein (YFP), in the presence or absence of an osmoticum (sorbitol) in time-course experiments (52). Whole seedlings were grown submerged in liquid culture (11), and the media was exchanged for fresh media containing the ISX solvent DMSO, sorbitol, Driselase, ISX, Driselase with

sorbitol, or ISX with sorbitol at the 0h time point. At 7h, epidermal cells in the root elongation zone of ISX-treated seedlings exhibited a swollen phenotype, which was reduced by co-treatment with sorbitol (fig. S1A). Driselase treatment resulted in degradation of the root tip (including the elongation zone) after 7h leaving behind only larger, already fully elongated cells for visualization (fig. S1B). This degradation was possibly enhanced by the addition of osmoticum. Because the effects on roots were so pronounced after 7h of treatment, we did not investigate the phenotypic effects in roots at later time points. In cotyledons of ISX-treated seedlings, the plasma membrane marker signal was similar to that in cotyledons from DMSO controls after 7h but was lost in patches after 24h (fig. S2A, B). Sorbitol treatment alone had no effect on membrane marker intensity, but, when co-administered with ISX, restored the marker signal at the 24h time point. Driselase treatment resulted in the formation of patches lacking the membrane marker after 7h (fig. S2C). These patches seemed to be more pronounced after 24h and were not affected by the addition of sorbitol (fig. S2C, D).

After establishing the dynamics of CWD responses we used the same experimental setup to investigate cell death and the deposition of lignin and callose in cotyledons and the accumulation of JA and SA in whole seedlings (11). We included also *isoxaben resistant1-1* (*ixr1-1*) and *bak1-5* mutant seedlings in the studies. The *ixr1-1* mutation causes an amino acid substitution in CELLULOSE SYNTHASE A3 (CESA3) that renders the protein resistant to inhibition by ISX (53), thus providing a control for ISX specificity. Plants carrying the *bak1-5* allele are only impaired in immune responses triggered by LRR-RLKs but not in brassinosteroid-dependent signaling, making the plants a suitable control for detecting the involvement of either DAMPs (for example *At*Pep1) generated by CWD or PAMPs that are

possibly present as contaminants in Driselase (54) and perceived by LRR-RLKs. Col-0 (wild-type) and *bak1-5* seedlings that were mock (DMSO)-treated or treated with boiled (inactivated) Driselase exhibited no cell death in cotyledons (fig. S3A, B). *ixr1-1* seedlings treated in the same manner exhibited a slight increase in cell death compared to Col-0. Treatment with ISX induced cell death in Col-0 and *bak1-5,* but not in *ixr1-1* cotyledons compared to mock-treated controls. Driselase treatment induced cell death in all genotypes examined. Sorbitol addition suppressed ISX-induced cell death but had no effect on Driselase-induced cell death.

We also analyzed compensatory lignin deposition in the cotyledons of seedlings that were treated with DMSO, ISX, boiled Driselase, or Driselase, with or without sorbitol, for 24h (fig. S3C). Lignin deposition was detectable after ISX treatment in vascular tissue areas in Col-0 and *bak1-5* but not in *ixr1-1* seedlings. Driselase-treated Col-0, *bak1-5,* and *ixr1-1* seedlings exhibited more ubiquitous lignin deposition. The addition of sorbitol reduced lignin deposition in all cases examined. *bak1-5* and *ixr1-1* cotyledons seemed more sensitive to Driselase treatment than Col-0 cotyledons based on cell death and lignin deposition phenotypes (fig. S3A, C).

Next we investigated compensatory callose deposition in the cotyledons of seedlings treated in the same manner. Whereas there was no detectable callose deposition in mock-treated or boiled Driselase–treated Col-0 and *bak1-5* cotyledons, callose was deposited in *ixr1-1* cotyledons subjected to these same control treatments (fig. S3D). Sorbitol alone had no effect on callose deposition in Col-0 and *bak1-5* cotyledons but reduced callose deposition in both *ixr1-1* treatment groups. ISX treatment induced callose deposition strongly in Col-0 seedlings, moderately in *bak1-5* seedlings, but not in *ixr1-1* seedlings. Sorbitol co-treatment

with ISX reduced callose deposition in Col-0 and *bak1-5*. Driselase treatment induced callose deposition in Col-0, but not in *bak1-5* cotyledons, and did not induce more callose deposition in *ixr1-1* seedlings than did boiled Driselase treatment (fig. S3D). *bak1-5* plants also exhibit reduced flg22-induced callose deposition, suggesting that the lack of induction observed here is part of a more general defect (55). The lack of significant increase in callose deposition in *ixr1-1* was possibly caused by the combination of the substantial amount of basal callose deposition in mock conditions and limited callose induction by Driselase.

We next quantified phytohormones in Col-0, *bak1-5*, and *ixr1-1* seedlings treated in the same manner as before. JA and SA abundances were low in mock-treated Col-0 and *bak1-5* seedlings and slightly increased in *ixr1-1* seedlings (Fig. 1A, B). ISX treatment induced JA accumulation in *bak1-5* seedlings more than in Col-0 seedlings, but no induction was observed in *ixr1-1* seedlings (Fig. 1A). ISX induced SA accumulation in both Col-0 and *bak1-5* seedlings to a similar degree, but not in *ixr1-1* seedlings (Fig. 1B). Co-treatment with sorbitol repressed ISX-induced JA and SA accumulation in Col-0 and *bak1-5*. Phytohormone amounts were lower in *ixr1-1* seedlings treated with sorbitol or a combination of ISX and sorbitol than in mock-treated *ixr1-1* seedlings, suggesting that sorbitol reduced stress in these plants (Fig. 1A, B). Driselase treatments induced JA and SA accumulation in Col-0, *bak1-5*, and *ixr1-1* seedlings to different degrees compared to treatment with boiled Driselase (Fig. 1C, D). In contrast to ISX treatments, Driselase treatment reduced SA accumulation in *bak1-5* compared to Col-0 (Fig. 1D). Although induction of both JA and SA by Driselase was less pronounced than induction by ISX in Col-0 and *bak1-5* (Fig. 1A–D), sorbitol co-treatments nevertheless reduced or prevented accumulation of JA and SA in all genotypes examined. The results of

these experiments suggest that responses to CWD are not restricted to a particular cell type (exemplified by lignin deposition in both vascular and epidermal tissues). Despite apparent differences in damage caused by ISX and Driselase, Col-0 seedlings exhibited similar osmo-sensitive responses to both types of CWD with respect to callose, lignin deposition as well as JA and SA accumulation. These observations suggest that both mechano- and osmo-perception may be required for induction of CWD responses. *bak1-5* seedlings, which have defects in PTI, exhibited distinct differences in their responses to the two CWD-inducing stimuli, suggesting some cross-regulation between PTI and CWI signaling.

Osmosensitivity distinguishes CWI signaling from DAMP- and PAMP-dependent responses

To investigate the regulatory processes responsible for the observed CWD-induced phenotypes, we first performed expression analysis of the defense marker *PLANT DEFENSIN1.2* (*PDF1.2*) because it encodes a defense peptide that is involved in both CWD- and PTI-mediated processes (37, 56). In both Col-0 and *bak1-5* seedlings, treatment with boiled or active Driselase induced *PDF1.2* expression; however, *PDF1.2* was less highly expressed in boiled Driselase–treated *bak1-5* seedlings compared to boiled Driselase–treated Col-0, and it was more highly induced by Driselase in *bak1-5* than in Col-0 seedlings (Fig. 1E). This supports the hypothesis that BAK1 might contribute to the PTI-mediated recognition of factors in the enzyme preparation, which are not removed by boiling, but represses the response to CWD elicited by the active enzymes. To investigate the role of mechanoperception in the response to CWD, we analyzed the expression of a marker for

mechanical stimulation (*TOUCH4*, *TCH4*) in ISX- and Driselase-treated Col-0 seedlings (57). ISX and active Driselase induced *TCH4* expression, whereas sorbitol co-treatments reduced it, providing support for an involvement of mechanoperception in the detection of CWD (Fig. 1F).

The results from the phytohormone measurements in *bak1-5* seedlings treated with ISX and Driselase with or without sorbitol, in conjunction with the results from the *PDF1.2* expression analysis, suggested that DAMP or PAMP signaling, or both, might also be sensitive to turgor changes. Therefore we investigated a possible involvement of OG-induced signaling in turgor-sensitive CWI maintenance using gene expression analysis and phytohormone measurements (58). We examined the expression of *RETICULIN OXIDASE* (*RET-OX*) and *CYTOCHROME P450*, *FAMILY 81*, *SUBFAMILY F*, *POLYPEPTIDE 2* (*CYP81F2*), both of which are induced by OG and the flagellin derivative flg22 (58), in Col-0 seedlings that had been treated with two different concentrations of OGs in the absence or presence of the osmoticum sorbitol. Expression of both genes was induced by OG treatments but was not sensitive to sorbitol co-treatment (fig. S4A, B). We also quantified JA and SA in seedlings treated in the same manner. Both OG and sorbitol treatments resulted in only minor changes in phytohormone amounts (fig. S4C, D). These results showed that OGs can be perceived by the seedlings in our assay and that OG-induced responses, unlike ISX- and Driselase-induced responses, are not osmosensitive, suggesting that CWD responses analyzed here do not involve OG-dependent signaling.

Next we quantified *RET-OX* and *CYP81F2* expression and the amounts of JA and SA in seedlings treated with flg22, sorbitol, or both flg22 and sorbitol. *RET-OX* and *CYP81F2*

expression was not significantly increased by sorbitol treatment alone, increased moderately by flg22 treatment, and increased greatly in seedlings treated with flg22 plus sorbitol (fig. S4E, F). Treatments with sorbitol and flg22 resulted in changes in JA amounts that were at the lower limit of detection, though both sorbitol alone and flg22 plus sorbitol promoted JA accumulation (fig. S4G). Flg22 induced SA accumulation after 3h and 7h of treatment, and co-treatment with sorbitol enhanced SA accumulation after 7h (fig. S4H). These results showed that flg22-induced gene expression, JA and SA accumulation are turgor-sensitive. However, sorbitol treatments seem to enhance the flg22-induced responses, contrary to what we observed with the responses to Driselase and ISX. These results suggest that turgor pressure is relevant for flg22-induced responses but that the underlying regulatory process is distinct from CWI maintenance signaling.

Isoxaben and cell wall–degrading enzymes induce similar osmosensitive responses

Driselase is a complex mix of enzymes that degrade several different cell wall polymers (59). To investigate whether the effects observed in Driselase-treated seedlings can be assigned to particular enzymatic activities, we obtained homogeneous preparations of the individual enzymes (xylanase, cellulase, pectinase) that, according to the manufacturer, account for the majority of the enzymatic activities in commercially-prepared Driselase. Initially we treated seedlings with increasing concentrations of the individual enzymes and measured phytohormone accumulation to establish optimal experimental conditions (fig. S5A, B). Xylanase did not induce phytohormone production, whereas cellulase induced only SA accumulation. Pectinase treatment increased the abundance of both SA and JA in seedlings in

a concentration-dependent manner. Based on these tests, we focused primarily on pectinase and cellulase. JA or SA did not accumulate in seedlings treated with boiled enzymes or sorbitol (fig. 1G-J). Pectinase treatment induced accumulation of both JA and SA in an osmosensitive manner (fig. 1G, H). Because cellulase treatment alone did not induce JA accumulation, we quantified hormone accumulation after combining cellulase with either xylanase or pectinase. Seedlings treated with cellulase plus xylanase exhibited no increase in JA and a moderate increase in SA accumulation, similar to cellulase alone (Fig. 1I, J and S5B). Cellulase plus pectinase elicited JA accumulation, which was higher than in the seedlings treated with the individual enzymes (Fig. 1G, I, S5A). SA amounts were lower than in pectinase-treated seedlings but higher than in those treated with cellulase alone (Fig. 1H, J, S5B). Sorbitol addition reduced phytohormone accumulation in all enzyme treatments examined. These results suggested that the combination of cellulase and pectinase is mainly responsible for the observed JA and SA accumulation in Driselase-treated seedlings. The differences in the effects of individual enzymes suggest that particular types of CWD may induce distinct phytohormone responses.

It is conceivable that a factor that is released or secreted from cells upon ISX or Driselase treatment is responsible for activation of the CWD responses observed. To test this hypothesis, we measured JA and SA accumulation in (i) *ixr1-1* seedlings that had been incubated with supernatants from Col-0 seedlings pre-treated with ISX for 12h or 24h and (ii) in Col-0 seedlings incubated with boiled supernatants from Col-0 seedlings pre-treated with Driselase for 12h or 24h (fig. S6A, B). JA accumulation was barely above the detection limit in the seedlings treated with the different supernatants (fig. S6C). With respect to SA

accumulation, only minor changes were detected compared to mock-treated samples (fig. S6D). These results suggested that ISX and Driselase treatments do not cause the release of a factor into the medium that is capable of inducing JA and SA accumulation. Taken together, the osmosensitivity and similarities in seedling responses to different types of CWD (enzymatic vs. ISX) suggest that different causes of CWD may stimulate cells similarly (or even in the same way), which in turn activates the same cellular responses.

Mechanical and hypo-osmotic stress sensors mediate certain CWD responses

The phenotypic data suggested that osmosensitive processes are an important element of the mechanism mediating CWD responses. Therefore we investigated whether genes implicated in the perception of mechanical [*MCA1*, *MECHANOSENSITIVE CHANNEL OF SMALL CONDUCTANCE* (*MSCS-LIKE*) *4 (MSL4), MSL5, MSL6, MSL9, and MSL10*)], hypo-osmotic *(MCA1, MSL2*, *MSL3*), and hyperosmotic stress [*ARABIDOPSIS HISTIDINE KINASE1 (AHK1*)*, AHK2 AHK3, AHK4*] were involved in CWI maintenance (17). We used plants harboring mutations in these genes and also included *the1-4* mutants in this analysis because *the 1-4* has been described as a gain-of-function allele that affects the cellular response to the inhibition of cellulose biosynthesis (20, 60). This allowed us to test whether any stimulus perceived by THE1 was also sensitive to osmoticum and to place osmosensitive responses upstream or downstream of THE1-mediated signaling. We treated mutant seedlings with ISX, sorbitol, or a combination of ISX plus sorbitol and measured JA accumulation in whole seedlings and lignification at the root tip (fig. S7A, B). JA and lignin were selected for this analysis because they enabled us to assess two qualitatively different

responses (phytohormone production and cell wall metabolism). For these experiments we used only ISX, because the analysis above had shown that JA accumulation and lignin production are activated similarly by ISX and Driselase in an osmosensitive manner. Only *mca1* and *msl2 msl3* seedlings exhibited reduced JA accumulation upon ISX treatment compared to the corresponding wild-type (Col-0 or Ws-2) controls (fig. S7A). ISX induced lignin deposition in all mutants and wild-type plants that were tested, but co-treatment with sorbitol reduced ISX-induced lignin accumulation (fig. S7B). Lignin deposition was reduced in *mca1* and enhanced in *msl4/5/6/9/10* (plants in which *MSL4*, *MSL5*, *MSL6*, *MSL9*, and *MSL10* were all mutated), *ahk1* and *ahk2 ahk3* seedlings compared to the corresponding controls (Fig. 2A). These results confirm the requirement of *MCA1* for ISX-induced JA and lignin accumulation (23) and indicate that *MSL2 MSL3* are required for JA accumulation whereas *MSL4*/*5*/*6*/*9*/*10*, *AHK1* and *AHK2 AHK3* only affect ISX-induced lignin production. In all genotypes examined (including *the1-4*) sorbitol co-treatments still reduced ISX-induced lignin and JA accumulation. This suggests that the effects of the sorbitol treatment could be due to turgor equilibration, illustrated by the shape changes in ISX-treated root epidermal cells (fig. S1A and previously reported in (61)) and would therefore not require any of the sensors tested (62). Turgor manipulation affects all the phenotypic effects of CWD that we examined, whereas supernatants from seedlings that had previously experienced CWD did not induce phytohormone production, the most sensitive readout of the response to CWD. This suggests that turgor-sensitive, non-secreted stimuli may activate CWD responses. The substantial accumulation of JA we observed in *the1-4* seedlings supports the hypothesis that the plasmamembrane-localized RLK THE1 is involved in perception of these turgor-sensitive

stimuli. This suggests that the stimuli indicating compromised CWI may consist of cell wall-bound epitopes that change conformation. Alternatively, mechanical distortion or displacement of the plasma membrane against the cell wall upon CWD, similar to the processes activating the CWI maintenance mechanism in *Saccharomyces cerevisiae*, are conceivable as stimuli (51).

Phenotypic clustering identifies a core group of RLKs and ion channels mediating CWI maintenance

Genes required for cell elongation, fertilization, and immunity have been implicated in CWI maintenance (3, 10, 19, 63). To gain further insight into the molecular mode of action of CWI maintenance and to establish which of the candidate genes are required and assess their relative importance in the process, we investigated knockout or gain-of-function alleles for 14 RLKs [*THE1*, *CURVY 1* (*CVY1*), *FER*, *HERCULES RECEPTOR KINASE 1* (*HERK1*), *HERK2*, *ERULUS* (*ERU*), *WAK2, FEI1*, *FEI2, MIK2*, *BAK1*, *BAK1-LIKE 1* (*BKK1*), *PEPR1*, *PEPR2*, *BIK1*, and *RECEPTOR-LIKE PROTEIN 44* (*RLP44*)]. The specific alleles of each gene, including a T-DNA insertion allele of *WAK2* that we designated as *WAK2-12* (fig. S8A-C), are noted in the figures and summarized in Table S2. We measured JA and SA accumulation in mock- and ISX-treated seedlings of these genotypes as well as in the osmosensing and mechanosensing *ahk1*, *ahk2* and *ahk3* (*ahk2/3*), *mca1*, *msl2* and *msl3* (*msl2/3*), and *msl4/5/6/9/10* mutants and in the ISX-resistant *ixr1* mutant (Fig. 2B, C and S9A-D). JA and SA accumulation was similar to the corresponding wild-type controls in all mock-treated genotypes with the exception of *fer-5* seedlings, which already exhibited increased JA and SA

accumulation in the mock-treated samples, in line with the multifunctional nature of FER (fig. S9A-D) (9, 64). Moreover, ISX-induced JA and SA accumulation were strongly increased in *fer-5* compared to wild-type, suggesting that *FER* is not essential for perception of ISX-induced CWD (fig. S9B, D). We also investigated root growth and ISX resistance, which could potentially distort the analyses performed here, in each genotype and found no substantial deviations from wild-type, with the exception of *bak1-5* seedlings showing somewhat shorter roots than wild-type seedlings and *irx1-1* seedlings being resistant to ISX, as expected. (fig. S9E, F). We quantified lignin deposition in the root tip area using an image analysis–based approach to generate quantitative data that could be normalized and used for subsequent hierarchical clustering (Fig. 2A). The quantitative data for JA, SA, and lignin accumulation were integrated through hierarchical clustering to generate a global, standardized overview, allowing assessment of both relative importance and functions of individual candidates in CWI maintenance (Fig. 2D). Data for *fer-5* were not included in the hierarchical clustering to avoid distortion during data integration due to the increased amounts of phytohormones in mock-treated seedlings (fig. S9A, C). The results showed that knockouts in five PTI signaling elements (*BAK1*, *BKK1*, *BIK1*, *PEPR1*, *PEPR2*) enhanced JA and SA accumulation in response to ISX treatment. Whereas the *WAK2*^{cTAP} dominant-active allele exhibited increased JA accumulation, *wak2* seedlings showed only a slight and statistically insignificant reduction in JA accumulation, which might be caused by redundancy within this gene family (8). In parallel, *fei2* and *mik2* seedlings exhibited significant reductions in the CWD responses examined, implicating (in the case of FEI2) or confirming (in the case of MIK2, (25)) their involvement in CWI maintenance. Seedlings in which the *Cr*RLK1L family members *CVY1*,

HERK1 and *HERK2* had been knocked out exhibited enhanced hormone responses, whereas *eru* seedlings were not strongly affected, and *the1-1* seedlings exhibited reduced responses, implying functional divergence within the *Cr*RLK1L family. Loss of *RLP44,* which is involved in cell wall-mediated activation of brassinosteroid signaling (63), did not affect the responses analyzed, suggesting that *RLP44* not required for responses to ISX-induced CWD. In summary, the hierarchical clustering showed that among the genes we tested *MIK2*, *MCA1*, *MSL2/3*, *FEI2*, and *THE1* are the most important ones for activation of ISX-induced CWD responses. Several of these proteins have been implicated in turgor- and mechano-perception and are located in the plasma membrane or plastid envelope, both of which are sub-cellular compartments that are particularly sensitive to changes in turgor and mechanical stimuli (19, 65).

THE1 is a key signaling element mediating CWD- but not PAMP-induced responses

We performed a genetic analysis to establish whether THE1, MCA1, and FEI2 are part of the same or different signaling cascade, using both a *THE1* loss-of-function (*the1-1*) and a gain-of-function (*the1-4*) allele. We generated the *mca1 fei2*, *the1-1 mca1*, *the1-1 fei2, the1-4 mca1*, and *the1-4 fei2* double mutants and measured the accumulation of JA, SA, and lignin in these mutant seedlings after mock and ISX treatments. JA, SA, and lignin phenotypes in *mca1 fei2*, *the1-1 mca1*, and *the1-1 fei2* seedlings were not additive, but *fei2* was epistatic to *mca1*, and *the1-1* was epistatic to both *mca1* and *fei2* (Fig. 3A-C). Next we compared responses in *the1-4 mca1* and *the1-4 fei2* seedlings to *the1-4* alone. JA and SA accumulation in the double mutants was reduced compared to *the1-4* and similar to Col-0, whereas relative lignification

was only reduced in *the1-4 mca1* (Fig. 3D-F). These results suggested that MCA1 and FEI2 are both required for hormone signaling downstream of THE1, but only MCA1 is required for THE1-dependent lignification.

Phenotypic clustering and genetic analyses confirmed THE1 as a key regulatory component in CWI maintenance in response to ISX treatment. To determine whether THE1 was also required for Driselase-induced CWD, we quantified JA and SA accumulation in *the1-1* loss-of-function and *the1-4* gain-of-function seedlings treated with boiled or active Driselase. SA content was slightly increased in *the1-4* controls treated with boiled Driselase compared to Col-0 seedlings, but JA content was similar in all genotypes (Fig. 3G, H). JA accumulation was reduced in *the1-1* and enhanced in *the1-4* seedlings upon treatment with active Driselase compared to Col-0 seedlings (Fig. 3G). SA amounts were increased similarly in Col-0 and *the1-4* seedlings compared to boiled Driselase controls, and even further increased in *the1-1* (Fig. 3H). These results suggest that a THE1-dependent mechanism controls JA accumulation in response to both Driselase- and ISX-induced CWD, but indicate that additional factors control SA accumulation in Driselase-treated seedlings.

THE1 is critical for CWI signaling and also involved in pathogen resistance (25). Therefore it is conceivable that THE1 might also be involved in PTI. We tested this by treating *the1-1* and *the1-4* seedlings with flg22 and measuring subsequently SA accumulation (fig. S10). SA accumulated similarly in Col-0, *the1-1*, and *the1-4* seedlings. In summary, these results suggest that THE1 acts upstream of MCA1 and FEI2, is required for both ISX and Driselase-induced JA production but is not required for PTI, implying that THE1 is specifically involved in CWI signaling.

AtPEP1 and AtPEP3 repress CWD-induced phytohormone production

To identify transcriptionally regulated elements of the CWI maintenance mechanism, Col-0 seedlings were mock- or ISX-treated and analyzed by RNA-Seq using mock- or ISX-treated *ixr1-1* seedlings as controls. In Col-0 seedlings treated with ISX for 1h, 109 transcripts exhibited statistically significant differences from mock-treated controls (Data file S1). Although mock-treated *ixr1-1* seedlings exhibited differences compared to mock-treated Col-0 at the transcriptome level, none of the ISX-regulated transcripts in Col-0 were differentially expressed in ISX-treated *ixr1-1* seedlings (Data file S1). GO enrichment analysis detected an over-representation of genes implicated in phytohormone-dependent stress responses in ISX-treated Col-0 seedlings (Table S1). Among the differentially expressed transcripts were *PROPEP1*, *PROPEP2*, *PROPEP3* and *PROPEP4*, which encode the precursors of the signaling peptides *At*Pep1–4 (fig. S11A) (43). PEPR1 has been shown to bind *At*Pep1–4, whereas PEPR2 binds only *At*Pep1 and *At*PEP2 (43). This observation was intriguing given that *pepr1* and *pepr2* seedlings exhibit enhanced JA accumulation upon ISX treatment (Fig. 2B). Gene expression analysis by qRT-PCR showed that *PROPEP1* and *PROPEP3* expression were particularly strongly induced by ISX (Fig. 4A). Time course expression analysis of *PROPEP1* and *PROPEP3* detected increases in expression over time in ISX-treated seedlings, suggesting that *At*Pep1 and *At*Pep3 might accumulate in response to ISX treatment (Fig. 4B). Expression of *PROPEP1* and *PROPEP3* was still increased in ISX-treated *the1-1* seedlings, indicating that their induction was independent of THE1-mediated processes (Fig. 4C). *At*Pep1 enhances JA, SA and ethylene accumulation in response to wounding (66).

To investigate whether *At*Pep1 also enhanced CWD responses, Col-0 seedlings were treated with different concentrations of *At*Pep1 alone or in combination with ISX before JA, SA, and lignin accumulation were measured. *At*Pep1 treatments alone did not induce JA and SA accumulation (Fig. 4D, E). Seedlings co-treated with ISX and *At*Pep1 exhibited reductions in ISX-induced JA and SA accumulation in a manner that depended on the concentration of *At*Pep1 (Fig. 4D, E). *At*Pep1 induced lignin deposition in Col-0 seedling roots in a distinctly different pattern than ISX treatment did whereas lignin deposition seemed to be additive in co-treated root tips compared to roots treated with either *At*Pep1 or ISX alone (fig. S11B).

To exclude indirect effects and determine whether the observed effects on *At*Pep1 were mediated by the established *At*Pep1 receptors, the experiments were repeated with Col-0, *pepr1*, *pepr2*, and *pepr1 pepr2* seedlings. ISX-induced JA and SA accumulation was reduced in *pepr1* and *pepr2* seedlings upon co-treatment with ISX and *At*Pep1, similarly to the Col-0 seedlings (Fig. 4F, G). However, this was not the case in *pepr1 pepr2* seedlings, in which co-treatment with *At*Pep1 did not counteract ISX-induced accumulation of JA and SA, suggesting that *At*Pep1 can inhibit ISX-induced phytohormone production through either PEPR1 or PEPR2. Analysis of lignin deposition in seedlings treated with *At*Pep1, ISX, or both *At*Pep1 and ISX showed that PEPR2 is essential for *At*Pep1-induced lignin deposition but PEPR1 is not (Fig. 4H). This provided further support for differences between PEPR1 and PEPR2 with respect to signaling activities. We also investigated *At*Pep3, which binds to PEPR1 but not to PEPR2, and found that *At*Pep3 co-treatment with ISX had similar effects as *At*Pep1 co-treatment on JA and SA accumulation in Col-0 seedlings (Fig. 4I, J). However, *At*Pep3 did not induce lignin production as did *At*Pep1 (fig. S11C), which can be explained by the inability of

*At*Pep3 to bind to PEPR2 (42). Because the fusion protein PROPEP3-Venus is secreted upon treatment with *At*Pep2 (67), we tested whether ISX treatment also induced PROPEP3-Venus secretion. Seedlings stably expressing *pPROPEP3*::PROPEP3-Venus were mock- or ISX-treated, and we immunoprecipitated the fusion protein from the growth medium (68). On a silver-stained polyacrylamide gel containing the protein preparations from the growth medium, bands of around 25 kDa were visible in preparations from both mock- and ISX-treated samples, consistent with the fusion protein being processed following secretion into the apoplast to release Venus alone (27 kDa) (Fig. 4K). A band corresponding to the size of the full-length fusion protein (PROPEP3-Venus, 37kDa) was only detected in the preparation from ISX-treated seedlings. Subjecting the proteins in these bands to peptide mass fingerprinting by liquid chromatography-coupled tandem mass spectrometry (LC-MS/MS) identified unique peptides corresponding to PROPEP3 and the VENUS tag with high confidence only in growth medium derived from ISX-treated seedlings (Fig. 4L, Data file S2). These results suggest that PROPEP3 is secreted from seedlings in response to ISX treatment.

Taken together, our data suggest that CWD induces the production of *At*Pep1 and *At*Pep3 through a mechanism that is independent of THE1 and seems to be regulated at the transcriptional level through controlled expression of *PROPEP1* and *PROPEP3*. The *At*Pep1 and 3 signaling process via PEPR1 and PEPR2 is redundantly organized because only *pepr1 pepr2* seedlings are unresponsive to *At*Pep1-treatment. *At*Pep1 and *At*Pep3 seem to act as inhibitors of phytohormone accumulation in response to CWD, whereas they have been previously described exclusively as enhancers of PTI responses. These results suggest that the specific activities of *At*Pep1 and *At*Pep3 are context-dependent.

Discussion

Here we have shown that two different types of CWD result in similar, osmosensitive responses in different cell types possible through a non-mobile stimulus, such as an alteration in a cell wall component, structure, or mechanical properties. We identified a small group of molecular components, most of which are involved in the perception of mechanical or hypo-osmotic stress, that mediate both local (deposition of lignin) and systemic (phytohormone accumulation) responses to CWD. Simultaneously we observed that loss of PTI signaling elements, such as BAK1, BIK1, BKK1, PEPR1, and PEPR2, enhanced the responses to CWD. We showed that THE1, MCA1, and FEI2 belong to the same signaling cascade and that THE1 was involved in mediating responses to both Driselase and ISX-induced CWD but not PTI-associated SA accumulation. We found that CWD induced *PROPEP1* and *PROPEP3* expression in a THE1-independent manner and that a PROPEP3-VENUS fusion protein is released into the growth medium from seedlings in response to ISX treatment. Application of *At*Pep1 and *At*Pep3 repressed CWD-induced JA and SA accumulation in a concentration-dependent manner, and repression by *At*Pep1 depended on the activity of PEPR1 and PEPR2. These results provide insights into the early events during CWD perception and the mechanisms regulating the cellular and systemic responses.

ISX and Driselase treatments resulted in similar responses in seedlings. Experiments with the individual cell wall–degrading enzymes found in Driselase and combinations thereof showed that pectinase and cellulase together caused overall the greatest JA accumulation, whereas SA amounts were lower than in seedlings treated with pectinase alone. Pectinase may increase the accessibility of cellulose to cellulase, thus facilitating the breakdown of this

load-bearing cell wall component, and perhaps explaining the similarities in the observed responses to ISX, Driselase, and combined pectinase plus cellulase treatments. Sorbitol co-treatments dampened all the responses to both enzyme- and ISX-induced CWD, suggesting that CWD responses are induced by a stimulus that is sensitive to turgor pressure. Treatments with supernatants derived from seedlings exposed to ISX or Driselase induced neither JA- nor SA-accumulation in a manner similar to Driselase and ISX treatments, suggesting that the stimulus activating the CWD responses is not mobile. All the genes that we identified through phenotypic clustering as being required for responses to CWD have been implicated in signal transduction or the perception of hypo-osmotic, mechanical, or cell wall damage (9, 19, 65, 69). This provides further support that the initial stimulus, indicating CWD has occurred, could be physical (mechanical). Taken together, these observations suggest that CWD could result in distortion or displacement of the plasma membrane relative to the cell wall possibly caused by changes in the surface tension of the wall itself due to weakening of the load-bearing cellulose framework. These changes in turn could be detected by the CWI maintenance mechanism and lead to the observed responses.

CWD in vivo is often caused by developmental processes, such as cell elongation, abiotic stressors, such as drought or cold temperature, or a pathogen breaking down the cell wall as part of the infection process (7, 70). Each of these different sources of CWD requires specialized, adaptive responses. The data presented here suggest that CWI and PTI signaling may coordinately contribute to these adaptive responses. If plants experience CWD, initially both CWI and *At*Pep-dependent PTI signaling seem to be activated independently (Fig. 5A). Induction of *PROPEP1* and *PROPEP3* expression leads to the release of PROPEPs, which

are probably processed in the apoplast to generate *At*Peps that are perceived by the receptors PEPR1 and PEPR2 and contribute to increased PTI responses (Fig. 5A, red elements). In parallel CWD is perceived separately through the CWI maintenance mechanism, which enables plant cells apparently to detect mechanical- or osmotic-induced physical damage to their cell walls or the consequences thereof (Fig. 5A, blue elements). If CWD is derived from developmental processes or abiotic stress, activation of the PROPEPs might not be further enhanced because PAMPs are absent, and the responses would consequently be mainly mediated by the CWI mechanism. If CWD is derived from a cell wall–degrading pathogen, PROPEP activation would be enhanced by the simultaneous presence of PAMPs (Fig. 5A). This leads on the one hand to increased activation of PTI-controlled, targeted defense responses and on the other hand to active repression of CWI-controlled responses through PEPR1 and PEPR2. If PTI is impaired - or if PEPR1 and PEPR2 are inactive - activation of the tailored defense responses is not enhanced, but the CWI-controlled responses are not repressed (Fig. 5B). This means that basal defense responses (exemplified here by JA and SA accumulation) controlled by the CWI maintenance mechanism are enhanced to compensate for a reduction of PTI controlled responses.

To summarize, the results presented here suggest that PTI and the CWI maintenance mechanism both “detect” CWD in plant cells in different ways and modulate responses in an adaptive manner. Coordination between PTI and CWI maintenance signaling is apparently mediated by *At*Pep1 and *At*Pep3, which function in this context as repressors, not enhancers, of CWI signaling. The effects observed in the *pepr1 pepr2* double-mutant seedlings suggest that the CWI maintenance mechanism acts as backup system for activating basal defenses in

case PTI and activation of the regular defense responses are impaired. Because homologs of THE1, MCA1, and WAK2 have been identified in both monocotyledonous and dicotyledonous plants as well as in more ancient species, the CWI maintenance mechanism - and potentially its interactions with PTI-based defense responses - may be conserved throughout the plant kingdom (28–30).

Materials and Methods

Reagents

All chemicals and enzymes were purchased from Sigma-Aldrich unless stated otherwise.

Plant growth and treatments

Wild-type and mutant *Arabidopsis thaliana* strains used in this study were ordered from the Nottingham Arabidopsis Stock Centre (http://arabidopsis.info/) or obtained directly from the laboratories previously publishing them. Detailed information is listed in Supplemental Table S2. Seedlings were grown in liquid culture as described (23) with minor modifications. Thirty milligrams of seeds were sterilized by sequential incubation with 70 % ethanol and 50 % bleach on a rotating mixer for 10 min each and washed 3 times with sterile water. Seeds were then transferred into 250 mL Erlenmeyer flasks containing 125 mL half-strength Murashige and Skoog growth medium (2.1 g/L Murashige and Skoog Basal Medium, 0.5 g/L MES salt and 1 % sucrose at pH 5.7). Seedlings were grown in long-day conditions (16h light, 22°C and 8h dark, 18°C) at 150 µmol m^{-2} s^{-1} photon flux density on a IKA KS501 flask shaker at a constant speed of 130 rotations per min.

For all experiments, seedlings were grown for 6 days before treatment. The following products were used for treatments at the indicated final concentrations throughout the manuscript, unless stated otherwise: Isoxaben (600 nM; DMSO), mock (DMSO), Driselase (0.03% w/v; Sigma D8037), cellulase (0.09% w/v; Duchefa C8001), pectinase (0.09% w/v; Sigma 17389), xylanase (0.09% w/v; Sigma X2753), sorbitol (300 mM). For heat inactivation, enzymes were boiled for 10 min. Supernatants from treated Col-0 cultures were incubated with *ixr1-1*

seedlings (DMSO, ISX, ISX+S) or boiled for 10 min and incubated with Col-0 seedlings (DMSO+S, bDri, bDri+S, Dri, Dri+S). *At*Pep1 (ATKVKAKQRGKEKVSSGRPGQHN), *At*Pep3 (EIKARGKNKTKPTPSSGKGGKHN), and flg22 (QRLSTGSRINSAKDDAAGLQIA) peptides were obtained from Peptron (Daejeon) and dissolved in sterile water.

Confocal Laser Scanning Microscopy

WAVE 131Y (52) seedlings used to investigate structural changes in root and cotyledon cells after cell wall damage were placed on microscopy slides, covered with the same medium used for the treatment and imaged with a Leica SP8 confocal laser scanning microscope (CLSM). Four Z-stacks were taken for each of the conditions analyzed using HC PL APO 10x/0.40 DRY objective (EX 514 nm, BA 525-535), pinhole 0.7 airy units (AU) and gain 700V. Z-stacks were transformed in 2D images by using the maximum intensity projections (0, threshold) function on LAS X software. To highlight the cell outlines, Z-projection images were transformed in gray-scale using GIMP v2.8.22 and presented as insets.

Phytohormone Analysis

The jasmonic acid (JA) and salicylic acid (SA) contents of seedlings were analyzed as described in (71) with minor modifications. Seedlings were sampled at 7h after treatment, flash-frozen in liquid nitrogen and freeze-dried for 24h. Aliquots each containing six to seven milligrams of freeze-dried seedlings were ground with 5 mm stainless steel beads in a Qiagen Tissue Lyser II for 2 min at 25 Hz. Shaking was repeated after the addition of 400 µL extraction buffer (10 % methanol, 1 % acetic acid) with internal standards (10 ng Jasmonic-d_5

Acid, 28 ng Salicylic-d_4 Acid; CDN Isotopes) before samples were incubated on ice for 30 min and centrifuged for 10 min at 16,000 g and 4°C. Supernatants were transferred into fresh tubes and the pellets were re-extracted with 400 µl extraction buffer without internal standards. Supernatants were combined and centrifuged 3 times to remove all debris prior to LC-MS/MS analysis. An extraction control not containing plant material was treated equally to the plant samples. Chromatographic separation was carried out on a Shimadzu UFLC XR, equipped with a Waters Cortecs C18 column (2.7 µm, 2.1 x 100 mm). The solvent gradient (acetonitrile (ACN) / water with 0.1 % formic acid each) was adapted to a total run time of 7 min: 0-4 min 20 % to 95 % ACN, 4-5 min 95 % ACN, 5-7 min 95 % to 20 % ACN; flow rate 0.4 ml / min. For hormone identification and quantification an AB SCIEX Triple Quad 5500 system was used. Mass transitions were: JA 209 > 59, D_5-JA 214 > 62, SA 137 > 93, D_4-SA 141 > 97.

Callose Analysis

Seedlings were sampled 24h after treatment and placed in 70 % (v/v) ethanol. For callose staining, samples were incubated in 0.07 M sodium phosphate buffer pH 9 for 30 min and in 0.005 % (w/v) aniline blue (in 0.07 M sodium phosphate buffer pH 9) for 60 min. Samples were washed with water, mounted in 50 % (v/v) glycerol and analyzed on a Nikon Eclipse E800 microscope using a UV-2A filter (EX 330-380 nm, DM 400 nm, BA 420 nm). Images were taken at 10x magnification and callose depositions quantified using ImageJ software.

Lignin Analysis

Lignification was investigated 12 h (root tips) and 24 h (cotyledons) after the start of

treatments. Lignin was detected with phloroglucinol-HCL as described (23). Seedlings were photographed using a Zeiss Axio Zoom.V16 stereomicroscope. To assess the extent of lignin production in root tips, phloroglucinol-stained areas and the total root area imaged were quantified using ImageJ (the same root length was maintained in all images taken). The relative lignified area was plotted as fold change compared to wild-type root tips.

Cell Death Analysis

Seedlings were sampled after 24h of treatment and incubated in trypan blue staining solution (0.025% trypan blue, 25% phenol, dissolved in equal volumes of lactic acid, glycerol, and water) for 6h at room temperature. Samples were de-stained in chloral hydrate overnight and transferred into 60% glycerol before microscopy. Images of the cotyledons were obtained with a Zeiss Axio Zoom.V16 stereomicroscope. The percentages of trypan blue-stained areas were quantified from cotyledons using ImageJ color thresholding.

Root Growth Measurements

Absolute root lengths were measured immediately prior to ISX treatment (0 h) to examine root growth phenotypes and 24h after start of treatment to determine ISX-dependent root growth inhibition (RGI). For calculation of %RGI the following formula was applied: [1 - (ISX 24h - ISX 0h) / (mock 24h - mock 0h)]*100.

Hierarchical Cluster Analysis

Hierarchical Clustering of ISX-dependent phenotypes was performed with Cluster 3.0 using

the C Clustering Library v1.52 (72). All data from mutant seedlings was normalized to their corresponding wild-type control. Log_2 transformed data was then used for average linkage clustering with an un-centered correlation similarity metric. Results were depicted using Java TreeView v1.1.6r4 and color-coded blue (less than in wild-type) or red (more than in wild-type) (73).

Genotyping the *WAK2* T-DNA insertion

Seeds were sown on a 6-well plate and grown in ½ MS1 for six days. Genomic DNA was extracted by grinding the plant material in a 2 mL Eppendorf tube with 5 mm stainless steel beads and 500 μL of extraction buffer (0,5 M NaCl, 50 mM EDTA, 0,1 M Tris-HCl, pH 8,0) in a Qiagen Tissue Lyser II for 1 min at 25 Hz. The lysate was centrifuged and 300 μL of supernatant was combined with 300 μL of isopropanol to precipitate the DNA. After centrifugation, the pellet was washed with 70% ethanol and dissolved in 100 μL of milli-Q water. One microliter of the isolated DNA was used for PCR reaction using Taq polymerase. The PCR program included an initial denaturation at 95 °C for 2 min followed by 30 cycles with 95 °C 30 s, 57 °C 30 s, 72 °C 1 min with final elongation at 72 °C for 2 min. The PCR products were run on 1% agarose gel containing Gel Red dye and imaged with a Syngene G-box imaging device.

qRT-PCR

Total RNA was isolated using a Spectrum Plant Total RNA Kit (Sigma-Aldrich). 2 micrograms of total RNA were treated with RQ1 RNase-Free DNase (Promega) and processed with the

ImProm-II Reverse Transcription System (Promega) for cDNA synthesis. qRT-PCR was performed using a LightCycler 480 SYBR Green I Master (Roche) and primers (Supplemental Table S3) diluted according to manufacturer specifications. Four different reference genes (*PP2A, ACT2, UBA1, GRF2*) were examined to identify one exhibiting stable expression during ISX-treatment. *ACT2* was the most stable and used in all experiments as a reference.

RNA-Seq Analysis

Total RNA was extracted using a Spectrum Plant Total RNA Kit (Sigma-Aldrich). RNA concentration was measured using a Qubit RNA HS Assay Kit (Thermo Fisher Scientific) and the integrity of the RNA assessed using an Agilent RNA 6000 Pico Kit. RNA Seq libraries were prepared using a TruSeq Stranded mRNA Kit (Illumina) according to the manufacturer's instructions. 500 ng total RNA was used as starting material.

First, index barcodes were ligated for identification of individual samples. mRNA purification, fragmentation, and cDNA synthesis was performed as described in (74). Exonuclease / polymerase was used to produce blunted overhangs. Illumina SR adapter oligonucleotides were ligated to the cDNA after 3' end adenylation. DNA fragments were enriched by 15 cycles of PCR reaction. The libraries were purified using the AMPure XP (Beckman Coulter), quantitated by qPCR using a KAPA Library Quantification Kit (Kapa Biosystems) and validated using a Agilent High Sensitivity DNA Kit on a Bioanalyzer. The size range of the DNA fragments were measured to be in the range of 200-700 bp and peaked around 296 bp. Libraries were normalized and pooled to 2.2 pM and subjected to clustering on NextSeq 500 high output flow cells. Finally, single-read sequencing was performed for 75 bp read lengths

on a NextSeq 500 instrument (Illumina) according to the manufacturer instructions. Base-calling has been performed on the NS500 instrument by Illumina RTA v2.4.6. FASTQ files were generated using bcl2fastq2 Conversion Software v1.8.4. Each FASTQ file was subjected to quality control trough fastQC v11.1 before technical replicates were combined and an average of 13.1 million reads was produced for each library. The reads were then aligned to the *A. thaliana* genome (Ensembl v82) with STAR v2.4.1 in two-pass mode. On average, 96.2% of the reads aligned to the genome. The reads that aligned uniquely to the genome were aggregated into gene counts with FeatureCounts v1.4.6 using the genome annotations defined in Ensembl v82. Of the 32000 genes defined in the gene model, a total of 20750 genes were left for analysis after filtering out genes with a CPM (counts-per-million) value less than one in two or more samples.

The filtered gene count table was used as input to the Voom method of the limma R package v3.26.9 for differential expression (75). The samples were normalized using the TMM method before a linear model was defined (76). Differential expression between groups were tested by empirical Bayesian moderated *t*-tests and *p*-values were corrected for multiple testing by the Benjamini-Hochberg false discovery rate (FDR) adjustment. Statistical significance of pairwise comparisons was determined using a Student's *t*-test. Genes with significantly altered expression after 1 h of ISX-treatment (Data File S1) were analyzed for GO enrichment using the PANTHER Overrepresentation Test (release 2016-07-15) and the GO Ontology database (Released 2017-02-28) on http://geneontology.org/. Results were filtered by $p < 0.05$ after Bonferroni correction for multiple testing. Data generated in the transcriptomics experiments are available under the following GEO submission ID: GSE109613.

Extracellular PROPEP3-Venus assay and peptide mass fingerprinting

Seedlings stably expressing *pPROPEP3*::PROPEP3-Venus were grown for 6 days prior to mock and ISX-treatment (68). After 24h, the growth medium was filtered through sterile miracloth and pH-adjusted to 7.5 with KOH. The number of seedlings per treatment was counted. Protease inhibitor cocktail (Sigma P9599) and phosphatase inhibitor cocktail 1 (Sigma P2850) were added to the medium. GFP-Trap agarose beads (Chromotek) were equilibrated according to manufacturer instructions and 50 µL bead slurry added to 2 mL medium. The suspension was tumbled end-over-end for 2h at 4°C. Beads were recovered by centrifugation and washed as described. Proteins were dissociated from beads by incubating 10 min at 95°C in 2x Laemmli buffer and supernatants separated via 10% Acrylamide gel for SDS-PAGE. Proteins were visualized using a Bio-Rad Silver Stain Plus Kit according to manufacturer instructions and the gel was imaged on a Bio-Rad ChemiDoc XRS+ System. Gel bands were cut in smaller pieces (3-5 mm^3) and were de-stained by incubation for 2 min in 150 µL ProteoSilver Destainer solution mix. The gel pieces were washed with ultrapure water and then shrunk with acetonitrile. They were reduced with DTT at 56°C, alkylated by iodoacetamide at room temperature in the dark, and – after being washed and shrunk – they were digested by trypsin at 37°C overnight. Peptides were collected, dried in a vacuum concentrator and reconstituted in 0.1% formic acid.

LC-MS/MS analysis was performed on an EASY-nLC 1200 UPLC system interfaced with an Q Exactive HF mass spectrometer via a Nanospray Flex ion source. Peptides were injected onto an Acclaim PepMap100 C18 trap column (75 µm i.d., 2 cm long, 3 µm, 100 Å) and further separated on an Acclaim PepMap100 C18 analytical column (75 µm i.d., 50 cm long, 2 µm,

100 Å) using a 60-min gradient (40 min 5-40 %B, 7 min 40-100 %B, 13 min 100 % B; where B is 0.1 % formic acid in CH3CN) at 250 nL/min flow. Peptides were analyzed in positive ion mode under data dependent acquisition (DDA) using the following parameters: Electrospray voltage 1.9 kV, HCD fragmentation with normalized collision energy 28. Each MS1 scan (200 to 2000 m/z, profile) was acquired at a resolution of 120,000 FWHM in the Orbitrap analyzer, followed by 15,000 FWHM MS2 scans (1.2 m/z isolation width, centroid) triggered for the 12 most intense ions, with a 15 s dynamic exclusion. Charge exclusion was set to unassigned, 1, and greater than 5.

Database search was performed in Proteome Discoverer 2.2 using Sequest HT engine against the proteome of Arabidopsis thaliana at UniProt (UP000006548, 2017-09-03), the amino acid sequence for PROPEP3-Venus and a list of sequences of usual protein contaminants. The search allowed up to 2 missed cleavages, precursor mass tolerance was 10 ppm and fragment mass tolerance was 0.02 Da. Carbamidomethyl (M +57.021 Da) was set as static modification and up to 4 dynamic modifications per peptide were allowed, possible modifications were: Oxidation (H,M,W +15.995 Da) and Deamidation (N,Q +0.984 Da). Validation was performed at PSM, Peptide and Protein level with high confidence set as 1% FDR and medium confidence representing 5% FDR. The mass spectrometry-derived proteomics data have been deposited to the ProteomeXchange Consortium via the PRIDE partner repository with the dataset identifier PXD009153 (77).

Statistical Analysis

Statistical significance was assed using either Student's *t*-test or one-way ANOVA followed by

post-hoc analysis with Tukey's HSD test. Statistical details of experiments are specified in the figure legends. Statistically significant differences are indicated by * $p < 0.05$, ** $p < 0.01$, *** $p < 0.001$ for Student's *t*-test and different letters for one-way ANOVA / Tukey's HSD test at $\alpha = 0.05$. All statistical analyses were performed in IBM SPSS Statistics v24.

Supplementary Materials

Data file S2: Peptide mass fingerprinting data

References and Notes

1. Höfte, H., and A. Voxeur. 2017. Plant cell walls. *Curr. Biol.* 27: R865–R870.

2. Somssich, M., G. A. Khan, and S. Persson. 2016. Cell Wall Heterogeneity in Root Development of Arabidopsis. *Front. Plant Sci.* 7: 1242.

3. Malinovsky, F. G., J. U. Fangel, and W. G. T. Willats. 2014. The role of the cell wall in plant immunity. *Front. Plant Sci.* 5: 178.

4. Hu, K., J. Cao, J. Zhang, F. Xia, Y. Ke, H. Zhang, W. Xie, H. Liu, Y. Cui, Y. Cao, X. Sun, J. Xiao, X. Li, Q. Zhang, and S. Wang. 2017. Improvement of multiple agronomic traits by a disease resistance gene via cell wall reinforcement. *Nat. plants* 3: 17009.

5. Shi, G., Z. Zhang, T. L. Friesen, D. Raats, T. Fahima, R. S. Brueggeman, S. Lu, H. N. Trick, Z. Liu, W. Chao, Z. Frenkel, S. S. Xu, J. B. Rasmussen, and J. D. Faris. 2016. The hijacking of a receptor kinase – driven pathway by a wheat fungal pathogen leads to disease. *Sci. Adv.* 2: 1–9.

6. Doblin, M. S., K. L. Johnson, J. Humphries, E. J. Newbigin, and A. T. Bacic. 2014. Are designer plant cell walls a realistic aspiration or will the plasticity of the plant's metabolism win out? *Curr. Opin. Biotechnol.* 26C: 108–114.

7. Wolf, S. 2017. Plant cell wall signalling and receptor-like kinases. *Biochem. J.* 474: 471–492.

8. Kohorn, B. D. 2016. Cell wall-associated kinases and pectin perception. *J. Exp. Bot.* 67: 489–94.

9. Nissen, K. S., W. G. T. Willats, and F. G. Malinovsky. 2016. Understanding CrRLK1L Function: Cell Walls and Growth Control. *Trends Plant Sci.* 21: 516–27.

10. Franck, C. M., J. Westermann, and A. Boisson-Dernier. 2018. Plant Malectin-Like Receptor Kinases: From Cell Wall Integrity to Immunity and Beyond. *Annu. Rev. Plant Biol.* 69: annurev-arplant-042817-040557.

11. Hamann, T., M. Bennett, J. Mansfield, and C. Somerville. 2009. Identification of cell-wall stress as a hexose-dependent and osmosensitive regulator of plant responses. *Plant J* 57: 1015–1026.

12. Manfield, I. W., C. Orfila, L. McCartney, J. Harholt, A. J. Bernal, H. V Scheller, P. M. Gilmartin, J. D. Mikkelsen, J. Paul Knox, and W. G. Willats. 2004. Novel cell wall architecture of isoxaben-habituated Arabidopsis suspension-cultured cells: global transcript profiling and cellular analysis. *Plant J* 40: 260–275.

13. Lorences, E. P., and S. C. Fry. 1994. Sequencing of xyloglucan oligosaccharides by partial Driselase digestion: The preparation and quantitative and qualitative analysis of two new tetrasaccharides. *Carbohydr. Res.* 263: 285–293.

14. Miedes, E., R. Vanholme, W. Boerjan, and A. Molina. 2014. The role of the secondary cell wall in plant resistance to pathogens. *Front. Plant Sci.* 5: 358.

15. Ferrari, S., D. V Savatin, F. Sicilia, G. Gramegna, F. Cervone, and G. De Lorenzo. 2013. Oligogalacturonides: plant damage-associated molecular patterns and regulators of growth and development. *Front. Plant Sci.* 4: 49.

16. Souza, C. de A., S. Li, A. Z. Lin, F. Boutrot, G. Grossmann, C. Zipfel, and S. C. Somerville. 2017. Cellulose-Derived Oligomers Act as Damage-Associated Molecular Patterns and Trigger Defense-Like Responses. *Plant Physiol.* 173: 2383–2398.

17. Hamant, O., and E. S. Haswell. 2017. Life behind the wall: sensing mechanical cues in

plants. *BMC Biol.* 15: 59.

18. Tateno, M., C. Brabham, and S. DeBolt. 2015. Cellulose biosynthesis inhibitors - a multifunctional toolbox. *J. Exp. Bot.* 67: 533–542.

19. Engelsdorf, T., and T. Hamann. 2014. An update on receptor-like kinase involvement in the maintenance of plant cell wall integrity. *Ann. Bot.* 114: 1339–47.

20. Hematy, K., P. E. Sado, A. Van Tuinen, S. Rochange, T. Desnos, S. Balzergue, S. Pelletier, J. P. Renou, and H. Hofte. 2007. A receptor-like kinase mediates the response of Arabidopsis cells to the inhibition of cellulose synthesis. *Curr Biol* 17: 922–931.

21. Feng, W., D. Kita, A. Peaucelle, H. N. Cartwright, V. Doan, Q. Duan, M.-C. Liu, J. Maman, L. Steinhorst, I. Schmitz-Thom, R. Yvon, J. Kudla, H.-M. Wu, A. Y. Cheung, and J. R. Dinneny. 2018. The FERONIA Receptor Kinase Maintains Cell-Wall Integrity during Salt Stress through Ca 2+ Signaling. *Curr. Biol.* 28: 666–675.

22. Nakagawa, Y., T. Katagiri, K. Shinozaki, Z. Qi, H. Tatsumi, T. Furuichi, A. Kishigami, M. Sokabe, I. Kojima, S. Sato, T. Kato, S. Tabata, K. Iida, A. Terashima, M. Nakano, M. Ikeda, T. Yamanaka, and H. Iida. 2007. Arabidopsis plasma membrane protein crucial for Ca2+ influx and touch sensing in roots. *Proc Natl Acad Sci U S A* 104: 3639–3644.

23. Denness, L., J. F. McKenna, C. Segonzac, A. Wormit, P. Madhou, M. Bennett, J. Mansfield, C. Zipfel, and T. Hamann. 2011. Cell wall damage-induced lignin biosynthesis is regulated by a reactive oxygen species- and jasmonic acid-dependent process in Arabidopsis. *Plant Physiol.* 156: 1364–74.

24. Kohorn, B. D., S. L. Kohorn, T. Todorova, G. Baptiste, K. Stansky, and M. McCullough. 2012. A dominant allele of Arabidopsis pectin-binding wall-associated kinase induces a stress

response suppressed by MPK6 but not MPK3 mutations. *Mol. Plant* 5: 841–51.

25. Van der Does, D., F. Boutrot, T. Engelsdorf, J. Rhodes, J. F. McKenna, S. Vernhettes, I. Koevoets, N. Tintor, M. Veerabagu, E. Miedes, C. Segonzac, M. Roux, A. S. Breda, C. S. Hardtke, A. Molina, M. Rep, C. Testerink, G. Mouille, H. Höfte, T. Hamann, and C. Zipfel. 2017. The Arabidopsis leucine-rich repeat receptor kinase MIK2/LRR-KISS connects cell wall integrity sensing, root growth and response to abiotic and biotic stresses. *PLoS Genet.* 13: e1006832.

26. Brutus, A., F. Sicilia, A. Macone, F. Cervone, and G. De Lorenzo. 2010. A domain swap approach reveals a role of the plant wall-associated kinase 1 (WAK1) as a receptor of oligogalacturonides. *Proc. Natl. Acad. Sci. U. S. A.* 107: 9452–9457.

27. Kamano, S., S. Kume, K. Iida, K.-J. Lei, M. Nakano, Y. Nakayama, and H. Iida. 2015. Transmembrane Topologies of Ca2+-permeable Mechanosensitive Channels MCA1 and MCA2 in Arabidopsis thaliana. *J. Biol. Chem.* 290: 30901–9.

28. Rosa, M., M. J. Abraham-Juarez, M. W. Lewis, J. P. Fonseca, W. Tian, V. Ramirez, S. Luan, M. Pauly, and S. Hake. 2017. The Maize MID-COMPLEMENTING ACTIVITY Homolog CELL NUMBER REGULATOR13/NARROW ODD DWARF Coordinates Organ Growth and Tissue Patterning. *Plant Cell* 29: 474–490.

29. Kurusu, T., D. Nishikawa, Y. Yamazaki, M. Gotoh, M. Nakano, H. Hamada, T. Yamanaka, K. Iida, Y. Nakagawa, H. Saji, K. Shinozaki, H. Iida, and K. Kuchitsu. 2012. Plasma membrane protein OsMCA1 is involved in regulation of hypo-osmotic shock-induced Ca2+ influx and modulates generation of reactive oxygen species in cultured rice cells. *BMC Plant Biol.* 12: 11.

30. Honkanen, S., V. A. S. Jones, G. Morieri, C. Champion, A. J. Hetherington, S. Kelly, H.

Proust, D. Saint-Marcoux, H. Prescott, and L. Dolan. 2016. The Mechanism Forming the Cell Surface of Tip-Growing Rooting Cells Is Conserved among Land Plants. *Curr. Biol.* 26: 3238–3244.

31. Du, S., L.-J. Qu, and J. Xiao. 2018. Crystal structures of the extracellular domains of the CrRLK1L receptor-like kinases ANXUR1 and ANXUR2. *Protein Sci.* 27: 886–892.

32. Kohorn, B. D., S. Johansen, A. Shishido, T. Todorova, R. Martinez, E. Defeo, and P. Obregon. 2009. Pectin activation of MAP kinase and gene expression is WAK2 dependent. *Plant J.* 60: 974–982.

33. Masachis, S., D. Segorbe, D. Turrà, M. Leon-Ruiz, U. Fürst, M. El Ghalid, G. Leonard, M. S. López-Berges, T. A. Richards, G. Felix, and A. Di Pietro. 2016. A fungal pathogen secretes plant alkalinizing peptides to increase infection. *Nat. Microbiol.* 1: 16043.

34. Tsang, D. L., C. Edmond, J. L. Harrington, and T. S. Nuhse. 2011. Cell Wall Integrity Controls Root Elongation via a General 1-Aminocyclopropane-1-Carboxylic Acid-Dependent, Ethylene-Independent Pathway. *Plant Physiol.* 156: 596–604.

35. Ellis, C., I. Karafyllidis, C. Wasternack, and J. G. Turner. 2002. The Arabidopsis mutant cev1 links cell wall signaling to jasmonate and ethylene responses. *Plant Cell* 14: 1557–1566.

36. Cano-Delgado, A. I., K. Metzlaff, and M. W. Bevan. 2000. The eli1 mutation reveals a link between cell expansion and secondary cell wall formation in Arabidopsis thaliana. *Development* 127: 3395–3405.

37. Ellis, C., and J. G. Turner. 2001. The Arabidopsis mutant cev1 has constitutively active jasmonate and ethylene signal pathways and enhanced resistance to pathogens. *Plant Cell* 13: 1025–1033.

38. Couto, D., and C. Zipfel. 2016. Regulation of pattern recognition receptor signalling in plants. *Nat. Rev. Immunol.* 16: 537–552.

39. Zhang, J., W. Li, T. Xiang, Z. Liu, K. Laluk, X. Ding, Y. Zou, M. Gao, X. Zhang, S. Chen, T. Mengiste, Y. Zhang, and J.-M. Zhou. 2010. Receptor-like cytoplasmic kinases integrate signaling from multiple plant immune receptors and are targeted by a Pseudomonas syringae effector. *Cell Host Microbe* 7: 290–301.

40. Chinchilla, D., C. Zipfel, S. Robatzek, B. Kemmerling, T. Nurnberger, J. D. Jones, G. Felix, and T. Boller. 2007. A flagellin-induced complex of the receptor FLS2 and BAK1 initiates plant defence. *Nature* 448: 497–500.

41. Heese, A., D. R. Hann, S. Gimenez-Ibanez, A. M. E. Jones, K. He, J. Li, J. I. Schroeder, S. C. Peck, and J. P. Rathjen. 2007. The receptor-like kinase SERK3/BAK1 is a central regulator of innate immunity in plants. *Proc. Natl. Acad. Sci. U. S. A.* 104: 12217–22.

42. Roux, M., B. Schwessinger, C. Albrecht, D. Chinchilla, A. Jones, N. Holton, F. G. Malinovsky, M. Tör, S. de Vries, and C. Zipfel. 2011. The Arabidopsis leucine-rich repeat receptor-like kinases BAK1/SERK3 and BKK1/SERK4 are required for innate immunity to hemibiotrophic and biotrophic pathogens. *Plant Cell* 23: 2440–55.

43. Bartels, S., and T. Boller. 2015. Quo vadis, Pep? Plant elicitor peptides at the crossroads of immunity, stress, and development. *J. Exp. Bot.* 66: 5183–5193.

44. Kohorn, B. D., M. Kobayashi, S. Johansen, H. P. Friedman, A. Fischer, and N. Byers. 2006. Wall-associated kinase 1 (WAK1) is crosslinked in endomembranes, and transport to the cell surface requires correct cell-wall synthesis. *J. Cell Sci.* 119: 2282–2290.

45. Hamann, T. 2012. Plant cell wall integrity maintenance as an essential component of biotic

stress response mechanisms. *Front. Plant Sci.* 3: 77.

46. Nühse, T. S. 2012. Cell wall integrity signaling and innate immunity in plants. *Front. Plant Sci.* 3: 280.

47. Kubicek, C. P., T. L. Starr, and N. L. Glass. 2014. Plant Cell Wall–Degrading Enzymes and Their Secretion in Plant-Pathogenic Fungi. *Annu. Rev. Phytopathol.* 52: 427–451.

48. Walton, J. D. 1994. Deconstructing the Cell Wall. *Plant Physiol* 104: 1113–1118.

49. Basham, H. ., and D. F. Bateman. 1974. Killing of plant cells by pectic enzymes: the lack of direct injuirous interaction between pectic enzymes and tehir soluble reaction products and plant cells. *Phytopathology* 65: 141–153.

50. Wormit, A., S. M. Butt, I. Chairam, J. F. McKenna, A. Nunes-Nesi, L. Kjaer, K. O'Donnelly, A. R. Fernie, R. Woscholski, M. C. L. Barter, and T. Hamann. 2012. Osmosensitive changes of carbohydrate metabolism in response to cellulose biosynthesis inhibition. *Plant Physiol.* 159: 105–17.

51. Levin, D. E. 2011. Regulation of cell wall biogenesis in Saccharomyces cerevisiae: the cell wall integrity signaling pathway. *Genetics* 189: 1145–75.

52. Geldner, N., V. Denervaud-Tendon, D. L. Hyman, U. Mayer, Y. D. Stierhof, and J. Chory. 2009. Rapid, combinatorial analysis of membrane compartments in intact plants with a multicolor marker set. *Plant J.* 59: 169–178.

53. Scheible, W. R., R. Eshed, T. Richmond, D. Delmer, and C. Somerville. 2001. Modifications of cellulose synthase confer resistance to isoxaben and thiazolidinone herbicides in Arabidopsis Ixr1 mutants. *Proc Natl Acad Sci U S A* 98: 10079–10084.

54. Schwessinger, B., M. Roux, Y. Kadota, V. Ntoukakis, J. Sklenar, A. Jones, and C. Zipfel.

2011. Phosphorylation-dependent differential regulation of plant growth, cell death, and innate immunity by the regulatory receptor-like kinase BAK1. *PLoS Genet.* 7: e1002046.

55. Prince, D. C., C. Drurey, C. Zipfel, and S. A. Hogenhout. 2014. The Leucine-Rich Repeat Receptor-Like Kinase BRASSINOSTEROID INSENSITIVE1-ASSOCIATED KINASE1 and the Cytochrome P450 PHYTOALEXIN DEFICIENT3 Contribute to Innate Immunity to Aphids in Arabidopsis. *Plant Physiol.* 164: 2207–2219.

56. Manners, J. M., I. A. Penninckx, K. Vermaere, K. Kazan, R. L. Brown, A. Morgan, D. J. Maclean, M. D. Curtis, B. P. Cammue, and W. F. Broekaert. 1998. The promoter of the plant defensin gene PDF1.2 from Arabidopsis is systemically activated by fungal pathogens and responds to methyl jasmonate but not to salicylic acid. *Plant Mol. Biol.* 38: 1071–80.

57. Braam, J., M. L. Sistrunk, D. H. Polisensky, W. Xu, M. M. Purugganan, D. M. Antosiewicz, P. Campbell, and K. A. Johnson. 1996. Life in a changing world: TCH gene regulation of expression and responses to environmental signals. *Physiol Plant* 98: 909–916.

58. Gravino, M., D. V. Savatin, A. Macone, and G. De Lorenzo. 2015. Ethylene production in *Botrytis cinerea*- and oligogalacturonide-induced immunity requires calcium-dependent protein kinases. *Plant J.* 84: 1073–1086.

59. Zabotina, O. A., U. Avci, D. Cavalier, S. Pattathil, Y.-H. Chou, S. Eberhard, L. Danhof, K. Keegstra, and M. G. Hahn. 2012. Mutations in Multiple XXT Genes of Arabidopsis Reveal the Complexity of Xyloglucan Biosynthesis. *Plant Physiol.* 159: 1367–1384.

60. Merz, D., J. Richter, M. Gonneau, C. Sanchez-Rodriguez, T. Eder, R. Sormani, M. Martin, K. Hématy, H. Höfte, and M.-T. Hauser. 2017. T-DNA alleles of the receptor kinase THESEUS1 with opposing effects on cell wall integrity signaling. *J. Exp. Bot.* 68: 4583–4593.

61. Hamann, T. 2015. The plant cell wall integrity maintenance mechanism-concepts for organization and mode of action. *Plant Cell Physiol.* 56: 215–23.

62. Lockhart, J. A. 1965. An analysis of irreversible plant cell elongation. *J. Theor. Biol.* 8: 264–275.

63. Wolf, S., D. van der Does, F. Ladwig, C. Sticht, A. Kolbeck, A.-K. Schürholz, S. Augustin, N. Keinath, T. Rausch, S. Greiner, K. Schumacher, K. Harter, C. Zipfel, and H. Höfte. 2014. A receptor-like protein mediates the response to pectin modification by activating brassinosteroid signaling. *Proc. Natl. Acad. Sci. U. S. A.* 111: 15261–6.

64. Stegmann, M., J. Monaghan, E. Smakowska-Luzan, H. Rovenich, A. Lehner, N. Holton, Y. Belkhadir, and C. Zipfel. 2017. The receptor kinase FER is a RALF-regulated scaffold controlling plant immune signaling. *Science* 355: 287–289.

65. Haswell, E. S., and P. E. Verslues. 2015. Perspectives on: The response to osmotic challenges: The ongoing search for the molecular basis of plant osmosensing. *J. Gen. Physiol.* 145: 389–394.

66. Huffaker, A., G. Pearce, N. Veyrat, M. Erb, T. C. J. Turlings, R. Sartor, Z. Shen, S. P. Briggs, M. M. Vaughan, H. T. Alborn, P. E. A. Teal, and E. A. Schmelz. 2013. Plant elicitor peptides are conserved signals regulating direct and indirect antiherbivore defense. *Proc. Natl. Acad. Sci. U. S. A.* 110: 5707–12.

67. Yamada, K., M. Yamashita-Yamada, T. Hirase, T. Fujiwara, K. Tsuda, K. Hiruma, and Y. Saijo. 2015. Danger peptide receptor signaling in plants ensures basal immunity upon pathogen-induced depletion of BAK1. *EMBO J.* 35: e201591807.

68. Ross, A., K. Yamada, K. Hiruma, M. Yamashita-Yamada, X. Lu, Y. Takano, K. Tsuda, and

Y. Saijo. 2014. The Arabidopsis PEPR pathway couples local and systemic plant immunity. *EMBO J.* 33: 62–75.

69. Kohorn, B. D., M. Kobayashi, S. Johansen, J. Riese, L. F. Huang, K. Koch, S. Fu, A. Dotson, and N. Byers. 2006. An Arabidopsis cell wall-associated kinase required for invertase activity and cell growth. *Plant J* 46: 307–316.

70. Tenhaken, R. 2014. Cell wall remodeling under abiotic stress. *Front Plant Sci* 5: 771.

71. Forcat, S., M. H. Bennett, J. W. Mansfield, and M. R. Grant. 2008. A rapid and robust method for simultaneously measuring changes in the phytohormones ABA, JA and SA in plants following biotic and abiotic stress. *Plant Methods* 4: 16.

72. de Hoon, M. J. L., S. Imoto, J. Nolan, and S. Miyano. 2004. Open source clustering software. *Bioinformatics* 20: 1453–4.

73. Saldanha, A. J. 2004. Java Treeview--extensible visualization of microarray data. *Bioinformatics* 20: 3246–8.

74. Ren, N., G. Gao, Y. Sun, L. Zhang, H. Wang, W. Hua, K. Wan, and X. Li. 2015. MicroRNA signatures from multidrug-resistant Mycobacterium tuberculosis. *Mol. Med. Rep.* 12: 6561–7.

75. Law, J. A., and S. E. Jacobsen. Establishing, maintaining and modifying DNA methylation patterns in plants and animals. *Nat Rev Genet* 11: 204–220.

76. Robinson, M., and A. Oshlack. 2010. A scaling normalization method for differential expression analysis of RNA-seq data. *Genome Biol.* 11: R25.

77. Vizcaíno, J. A., A. Csordas, N. del-Toro, J. A. Dianes, J. Griss, I. Lavidas, G. Mayer, Y. Perez-Riverol, F. Reisinger, T. Ternent, Q.-W. Xu, R. Wang, and H. Hermjakob. 2016. 2016 update of the PRIDE database and its related tools. *Nucleic Acids Res.* 44: D447–D456.

78. Wohlbach, D. J., B. F. Quirino, and M. R. Sussman. 2008. Analysis of the Arabidopsis histidine kinase ATHK1 reveals a connection between vegetative osmotic stress sensing and seed maturation. *Plant Cell* 20: 1101–1117.

79. Higuchi, M., M. S. Pischke, A. P. Mahonen, K. Miyawaki, Y. Hashimoto, M. Seki, M. Kobayashi, K. Shinozaki, T. Kato, S. Tabata, Y. Helariutta, M. R. Sussman, and T. Kakimoto. 2004. In planta functions of the Arabidopsis cytokinin receptor family. *Proc. Natl. Acad. Sci. U. S. A.* 101: 8821–8826.

80. Veronese, P., H. Nakagami, B. Bluhm, S. Abuqamar, X. Chen, J. Salmeron, R. A. Dietrich, H. Hirt, and T. Mengiste. 2006. The Membrane-Anchored BOTRYTIS-INDUCED KINASE1 Plays Distinct Roles in Arabidopsis Resistance to Necrotrophic and Biotrophic Pathogens. *Plant Cell* 18: 257–273.

81. Gachomo, E. W., L. Jno Baptiste, T. Kefela, W. M. Saidel, and S. O. Kotchoni. 2014. The Arabidopsis CURVY1 (CVY1) gene encoding a novel receptor-like protein kinase regulates cell morphogenesis, flowering time and seed production. *BMC Plant Biol.* 14: 221.

82. Bai, L., Y. Zhou, X. Ma, L. Gao, and C.-P. Song. 2014. Arabidopsis CAP1-mediated ammonium sensing required reactive oxygen species in plant cell growth. *Plant Signal. Behav.* 9: e29582.

83. Haruta, M., G. Sabat, K. Stecker, B. B. Minkoff, and M. R. Sussman. 2014. A Peptide Hormone and Its Receptor Protein Kinase Regulate Plant Cell Expansion. *Science* 343: 408–411.

84. Xu, S.-L., A. Rahman, T. I. Baskin, and J. J. Kieber. 2008. Two leucine-rich repeat receptor kinases mediate signaling, linking cell wall biosynthesis and ACC synthase in

Arabidopsis. *Plant Cell* 20: 3065–79.

85. Duan, Q., D. Kita, C. Li, A. Y. Cheung, and H.-M. Wu. 2010. FERONIA receptor-like kinase regulates RHO GTPase signaling of root hair development. *Proc. Natl. Acad. Sci. U. S. A.* 107: 17821–6.

86. Guo, H., L. Li, H. Ye, X. Yu, A. Algreen, and Y. Yin. 2009. Three related receptor-like kinases are required for optimal cell elongation in Arabidopsis thaliana. *Proc. Natl. Acad. Sci. U. S. A.* 106: 7648–53.

87. Haswell, E. S., and E. M. Meyerowitz. 2006. MscS-like proteins control plastid size and shape in Arabidopsis thaliana. *Curr. Biol.* 22: 408-413.

88. Haswell, E. S., R. Peyronnet, H. Barbier-Brygoo, E. M. Meyerowitz, and J.-M. Frachisse. 2008. Two MscS homologs provide mechanosensitive channel activities in the Arabidopsis root. *Curr. Biol.* 18: 730–4.

89. Yamaguchi, Y., A. Huffaker, A. C. Bryan, F. E. Tax, and C. A. Ryan. 2010. PEPR2 is a second receptor for the Pep1 and Pep2 peptides and contributes to defense responses in Arabidopsis. *Plant Cell* 22: 508–522

90. Czechowski T, Stitt M, Altmann T, Udvardi MK and Scheible WR. 2005. Genome-wide identification and testing of superior reference genes for transcript normalization in Arabidopsis. *Plant Physiol.* 139: 5-17.

91. Sessions A, Burke E, Presting G, Aux G, McElver J, Patton D, Dietrich B, Ho P, Bacwaden J, Ko C, Clarke JD, Cotton D, Bullis D, Snell J, Miguel T, Hutchison D, Kimmerly B, Mitzel T, Katagiri F, Glazebrook J, Law M and Goff SA. 2002. A high-throughput Arabidopsis reverse genetics system. *Plant Cell* 14: 2985-94.

Acknowledgements: The authors would like to thank Davi de Miranda Fonseca and the NTNU Proteomics and Metabolomics Core Facility (PROMEC) for support with protein and hormone analysis; the NTNU Genomics Core Facility (GCF) for support with RNA-Sequencing; Giulia De Lorenzo (University of Rome) for providing oligogalacturonides, Yusuke Saijo and colleagues at the Nara Institute for Science and Technology for making available transgenic plant lines. We are grateful to Martin Kuiper and John Mansfield for constructive comments on the manuscript. **Funding**: Financial support from the Deutsche Forschungsgemeinschaft EN 1071/1-1, HORIZON2020 (SugarOsmoSignaling) (T.E.), BBSRC (J.F. McK.), NTNU (M.V.), the Norwegian Financial Mechanism 2009-2014 Project Contract no. MSMT-23681/2015-1 (N.G.B./T.H.), the Gatsby Charitable Foundation (C.Z.), and the European Molecular Biology Organization (ALTF 657-2013) (D.V.d.D.)are gratefully acknowledged. **Author contributions**: T.E., N.GB., M.V., L.V., T.H. contributed to experimental design, generated data and co-wrote the manuscript. J. McK. and F.A. contributed with experimental data. D.VdD. and C.Z. provided unpublished resources and contributed to the writing of the manuscript. **Competing interests**: The authors have no competing of interests. **Data and materials availability**: Data generated in the transcriptomics experiments have been deposited in the Gene Expression Omnibus (GEO, https://www.ncbi.nlm.nih.gov/geo/) with the identifier GSE109613. The mass spectrometry proteomics data have been deposited to the ProteomeXchange Consortium through the PRIDE partner repository (https://www.ebi.ac.uk/pride/archive/) with the dataset identifier PXD009153 (77).

Figure Legends

Fig. 1. Different types of cell wall damage induce similar osmosensitive responses. Quantification of (**A**) jasmonic acid (JA) and (**B**) salicylic acid (SA), expressed as μg per g dry weight (gDW), in Col-0, *bak1-5*, and *ixr1-1* seedlings that had been treated with DMSO (mock), DMSO and sorbitol (S), isoxaben (ISX), or isoxaben and sorbitol (ISX+S). (**C**) JA and (**D**) SA quantification in Col-0, *bak1-5*, and *ixr1-1* seedlings treated with boiled (inactive) Driselase (bDri), bDri and sorbitol (bDri+S), Driselase (Dri) or Driselase and sorbitol (Dri+S). (**E**) Relative expression of *PDF1.2* as dertermined by qRT-PCR in Col-0 and *bak1-5* seedlings treated with bDri or Dri compared to untreated (NT) seedlings. (**F**) Relative expression of *TCH4* in Col-0 seedlings treated as indicated. (**G**) JA and (**H**) SA quantification in Col-0 seedlings treated with boiled pectinase (bP), boiled pectinase and sorbitol (bP+S), pectinase (P), or pectinase and sorbitol (P+S). (**I**) JA and (**J**) SA quantification in Col-0 seedlings treated with the indicated combinations of boiled (b) or active preparations of cellulase (C), pectinase (P), xylanase (X), and sorbitol (S). All values represent means with error bars indicating SD. N = 4 (A–D), N = 3 (E–J). Letters a-d (A-J) indicate statistically significant differences according to one-way ANOVA and Tukey's HSD test ($\alpha = 0.05$) between treatments for each genotype. Asterisks (A–D) indicate statistically significant differences to the WT (Student's *t*-test; ** $p < 0.01$; *** $p < 0.001$; ns, not significant).

Fig. 2. Phenotypic clustering identifies groups of genes involved in cell wall damage responses. Quantification of (**A**) root tip lignification, (**B**) jasmonic acid (JA) and (**C**) salicylic acid (SA) in the indicated mutant seedlings after treatment with isoxaben (ISX). Values

represent means with error bars indicating SD and are expressed relative to the appropriate wild-type (WT) control (Col-0 or Ws-2, depending on the genetic background of the mutant strain) from a representative experiment (dashed line). N ≥ 10 (A). N = 4 (B, C); Asterisks indicate statistically significant differences between the mutant and WT (Student's *t*-test, * $p < 0.05$). Mutant lines are organized in functional groups (RLKs, Receptor-like kinases; *Cr*RLK1Ls, *Catharanthus roseus* RLK1-like kinases; AHKs, *Arabidopsis* histidine kinases; Ion channels), and individual genotypes described in detail in Supplemental Table S2. (**D**) Hierarchical clustering of mutant phenotypes assigning functions in CWI maintenance to candidate genes based on their responses to ISX. Mutant phenotype data from (A–C) and fig. S9F (RGI, root growth inhibition) were normalized to WT controls and $\log_2$ transformed prior to average linkage clustering. Blue color indicates reduced ISX responses, and red color indicates increased ISX responses compared to WT.

Fig. 3. THE1 functions upstream of MCA1 and FEI2 and promotes responses to different types of cell wall damage. Quantification of (**A**) root tip lignification, (**B**) jasmonic acid (JA) and (**C**) salicylic acid (SA) following ISX treatment in wild-type (Col-0) and mutant seedlings carrying the indicated loss-of-function mutations. Quantification of (**D**) root tip lignification, (**E**) JA, and (**F**) SA following ISX treatment in Col-0 and mutant seedlings carrying the gain-of-function allele *the1-4* or *the1-4* in combination with the loss-of-function alleles *mca1* or *fei2*. Quantification of (**G**) JA and (**H**) SA in Col-0, *the1-1* (loss-of-function), and *the1-4* (gain-of-function) seedlings treated with boiled Driselase (bDri) or Driselase (Dri). N ≥ 17 (lignin), N = 4 (JA, SA).. Letters a-e (A–F) indicate statistically significant differences between genotypes

according to one-way ANOVA and Tukey's HSD test (α = 0.05). Asterisks (G, H) indicate statistically significant differences compared to the Col-0 control (Student's *t*-test; * $p < 0.05$; ** $p < 0.01$; *** $p < 0.001$).

Fig. 4. Isoxaben induces *PROPEP* expression, and *At*Pep1 and *At*Pep3 repress responses to cell wall damage. (**A**) Relative *PROPEP1, PROPEP2, PROPEP3* and *PROPEP4* expression determined by qRT-PCR in Col-0 seedlings treated with DMSO (mock) or isoxaben (ISX) for 1 h. (**B**) *PROPEP1* and *PROPEP3* expression in Col-0 seedlings at the indicated time points. (**C**) *PROPEP1* and *PROPEP3* expression in Col-0 and *the1-1* seedlings after 1 h of mock or ISX treatment. Quantification of (**D**) jasmonic acid (JA) and (**E**) salicylic acid (SA) in Col-0 seedlings after co-treatment with either mock conditions or ISX plus 0, 1, 10, or 100 nM *At*Pep1. Quantification of (**F**) JA and (**G**) SA in Col-0, *pepr1*, *pepr2*, and *pepr1 pepr2* seedlings after co-treatment with either mock conditions or ISX plus 10 nM *At*Pep1. (**H**) Root tip lignification in Col-0, *pepr1*, *pepr2*, and *pepr1 pepr2* seedlings after co-treatment with either mock conditions or ISX plus 10 nM *At*Pep1 was visualized by phloroglucinol staining. Scale bar, 200 µm. Quantification of (**I**) JA and (**J**) SA in Col-0 seedlings after co-treatment with either mock conditions or ISX plus 0 or 10 nM *At*Pep3. All values represent means with error bars indicating SD. N = 3 (A–C, I–J), N = 4 (D–G), N ≥ 5 (H). Asterisks (A–C) indicate statistically significant differences compared to mock-treated controls (Student's *t*-test; * $p < 0.05$). Letters a–e (D–J) indicate statistically significant differences between treatments of each genotype according to one-way ANOVA and Tukey's HSD test (α = 0.05).

(**K**) Seedlings expressing PROPEP3-Venus were mock- or ISX-treated for 24 h. Proteins in the growth medium were immunoprecipitated, separated by SDS-PAGE, and stained with silver nitrate. The expected mass of PROPEP3-Venus is 37kDa, and the expected mass of Venus alone is 27kDa. N = 2. (**L**) Numbers of unique PROPEP3-Venus peptides after trypsin digest identified by LC-MS/MS from silver-stained bands at around 25 kDa and 37 kDa. FDR, false discovery rate.

Fig. 5. Model of stress response integration through CWI and PTI signaling. (**A**) Responses to cell wall damage caused by inhibition of cellulose biosynthesis (isoxaben, ISX) or enzymatic cell wall degradation (Driselase) in *Arabidopsis* depend on the receptor-like kinase (RLK) THE1. THE1 acts upstream of the ion channel MCA1 and the RLK FEI2 to stimulate the cell wall integrity (CWI) maintenance system. Independently, through an unknown mechanism, ISX treatment induces the expression of *PROPEP1* and *PROPEP3* (*PROPEP1/3*) and secretion of PROPEP3. Processing of PROPEP1 and PROPEP3 generate the host defense peptides *At*Pep1 and *At*Pep3 (*At*Pep1/3), which are damage-associated molecular patterns (DAMPs) that are also induced by pathogen elicitors during pattern-triggered immunity (PTI). *At*Pep1/3 repress ISX-induced hormone accumulation through the *At*Pep receptors PEPR1 and PEPR2, suggesting an *At*Pep-dependent negative feedback mechanism. *At*Pep signaling also induces a positive feedback loop that enhances PTI. (**B**) If PTI-mediated induction of *At*Peps or *At*Pep signaling is impaired, suppression of CWI signaling is alleviated, and the CWI maintenance pathway contributes to stress response induction to a greater extent than does PTI.

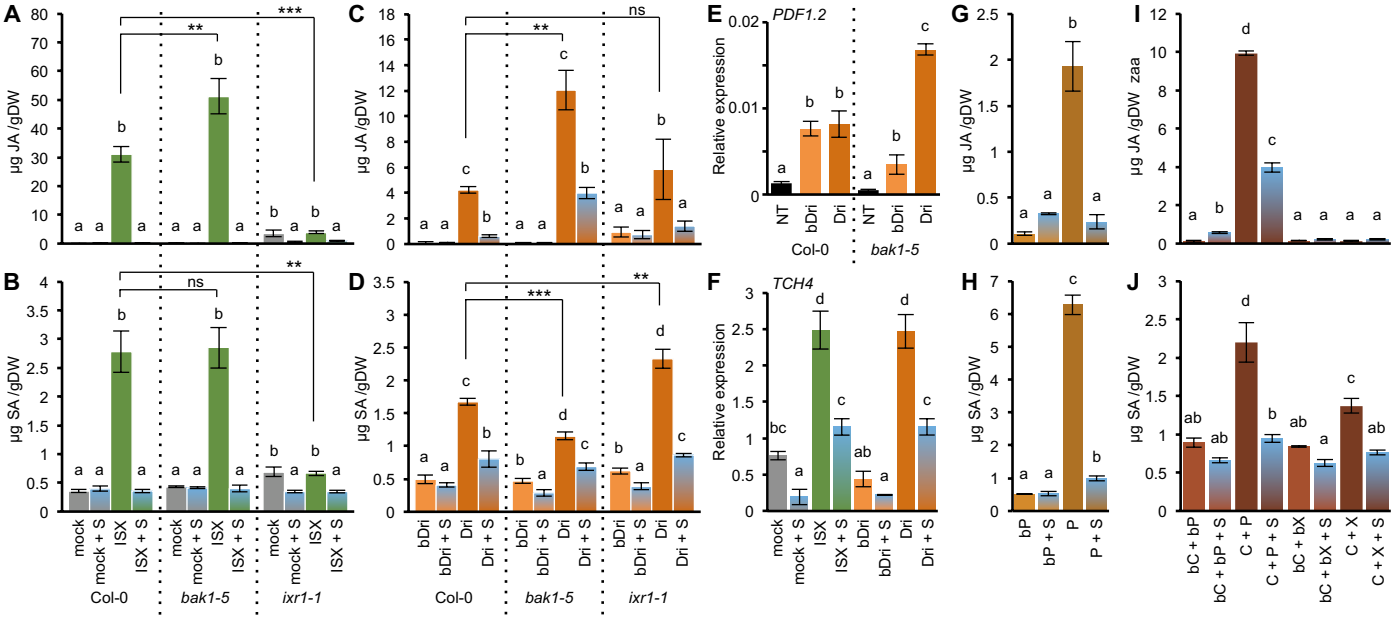
A
µg JA /gDW
mock
mock + S
ISX
ISX + S
Col-0
bak1-5
ixr1-1
B
µg SA /gDW
C
µg JA /gDW
bDri
bDri + S
Dri
Dri + S
D
µg SA /gDW
E
PDF1.2
Relative expression
NT
bDri
Dri
F
TCH4
G
µg JA /gDW
bP
bP + S
P
P + S
H
µg SA /gDW
I
µg JA /gDW zaa
bC + bP
bC + bP + S
C + P
C + P + S
bC + bX
bC + bX + S
C + X
C + X + S
J
µg SA /gDW

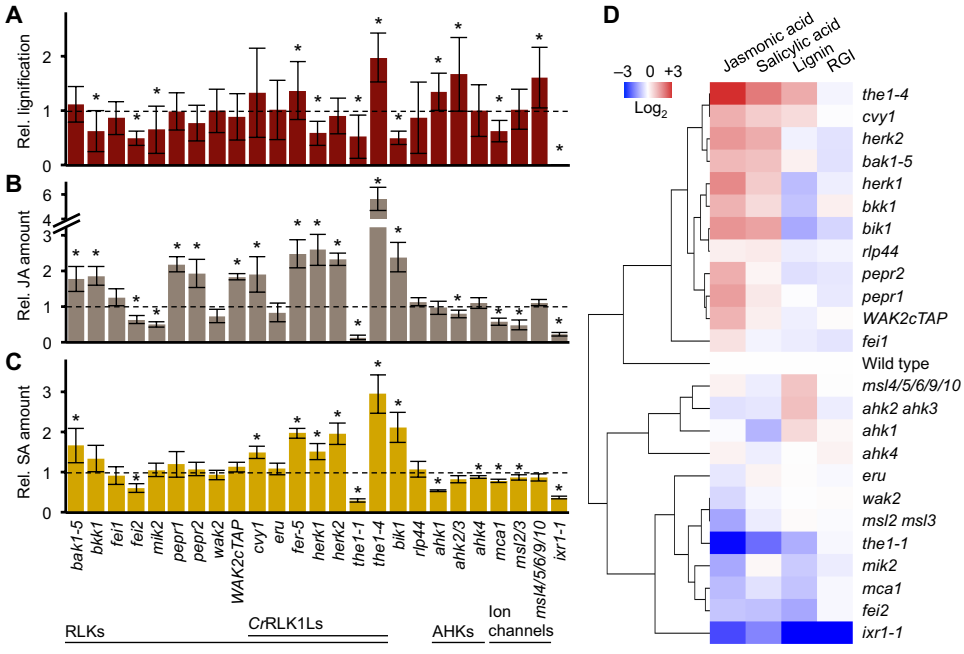
A
Rel. lignification
B
Rel. JA amount
C
Rel. SA amount
bak1-5
bkk1
fei1
fei2
mik2
pepr1
pepr2
wak2
WAK2cTAP
cvy1
eru
fer-5
herk1
herk2
the1-1
the1-4
bik1
rlp44
ahk1
ahk2/3
ahk4
mca1
msl2/3
msl4/5/6/9/10
ixr1-1
RLKs
CrRLK1Ls
AHKs
Ion channels
D
−3 0 +3
Log2
Jasmonic acid
Salicylic acid
Lignin
RGI
the1-4
cvy1
herk2
bak1-5
herk1
bkk1
bik1
rlp44
pepr2
pepr1
WAK2cTAP
fei1
Wild type
msl4/5/6/9/10
ahk2 ahk3
ahk1
ahk4
eru
wak2
msl2 msl3
the1-1
mik2
mca1
fei2
ixr1-1

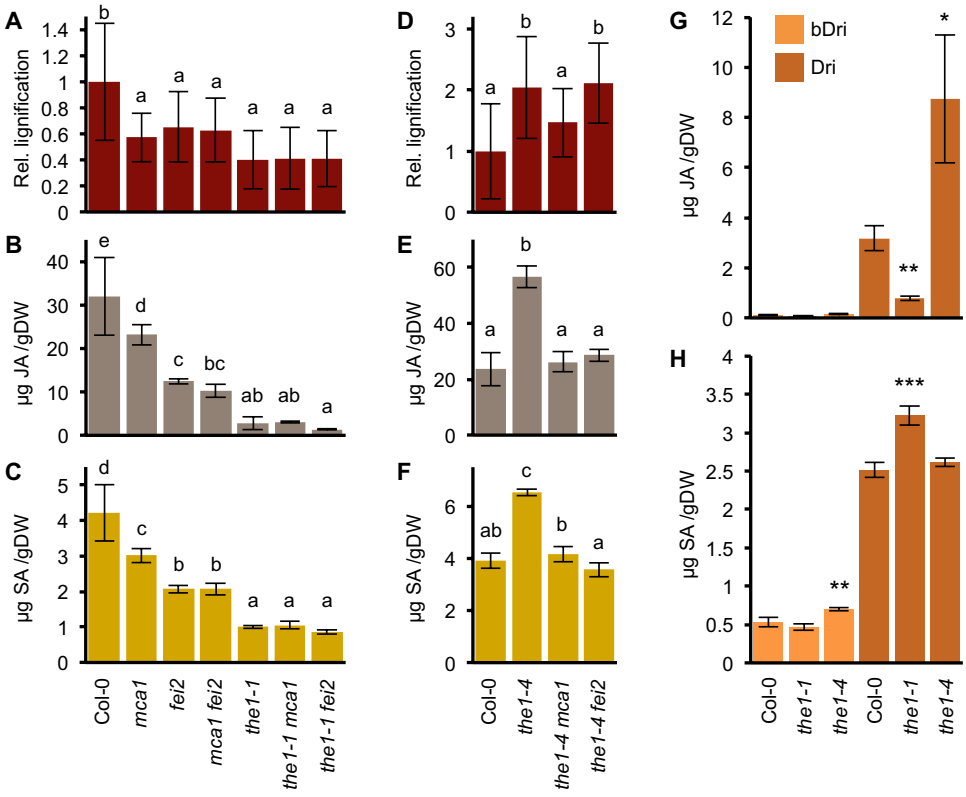
A
Rel. lignification
B
µg JA /gDW
C
µg SA /gDW
Col-0
mca1
fei2
mca1 fei2
the1-1
the1-1 mca1
the1-1 fei2
D
Rel. lignification
E
µg JA /gDW
F
µg SA /gDW
Col-0
the1-4
the1-4 mca1
the1-4 fei2
G
bDri
Dri
µg JA /gDW
H
µg SA /gDW
Col-0
the1-1
the1-4
Col-0
the1-1
the1-4

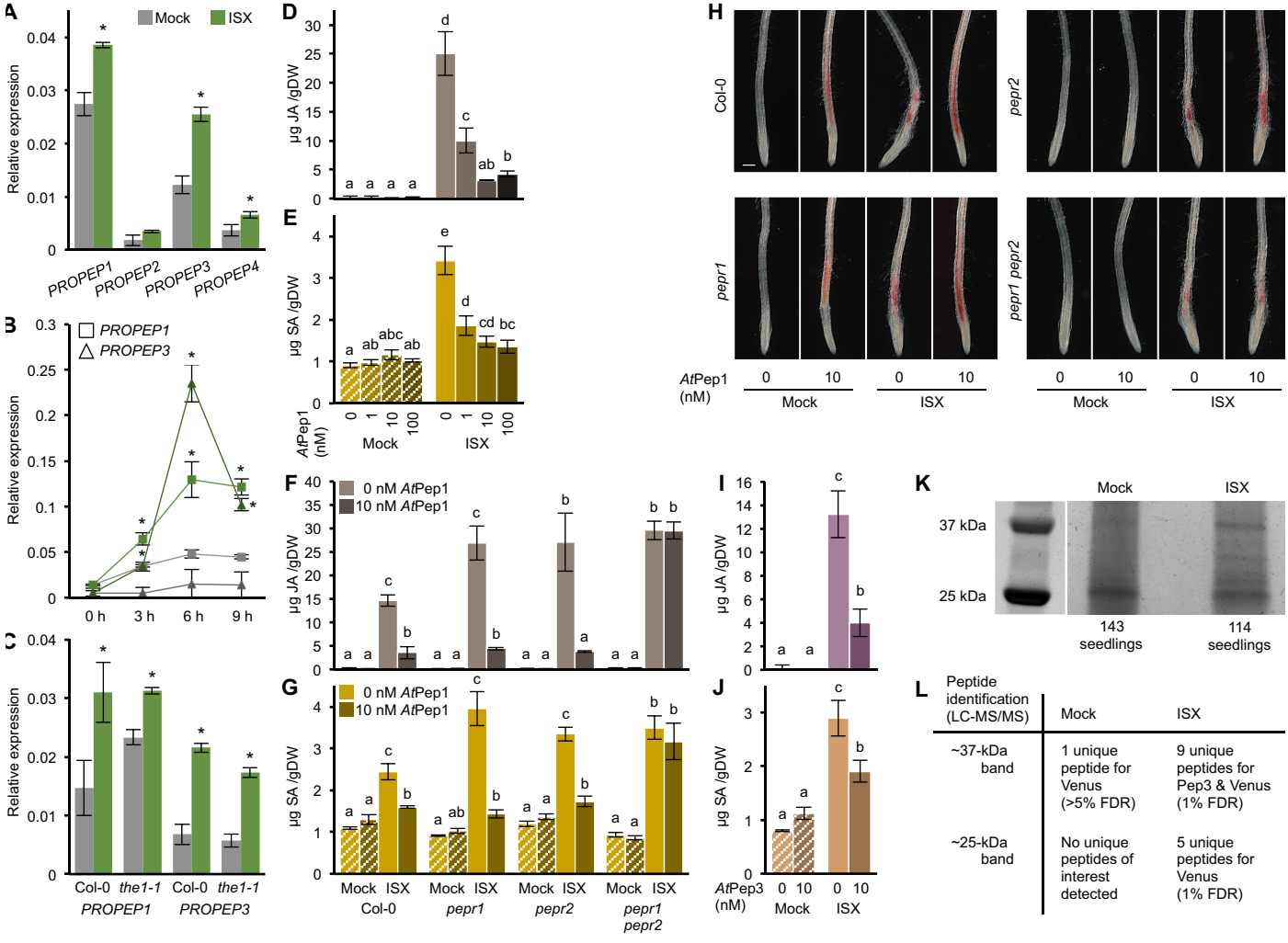

L

Peptide identification (LC-MS/MS)	Mock	ISX
~37-kDa band	1 unique peptide for Venus (>5% FDR)	9 unique peptides for Pep3 & Venus (1% FDR)
~25-kDa band	No unique peptides of interest detected	5 unique peptides for Venus (1% FDR)

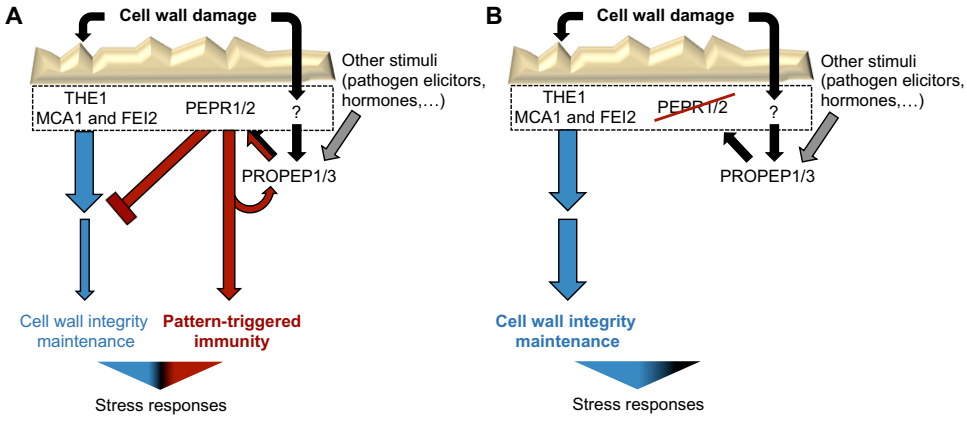
A
Cell wall damage
Other stimuli
(pathogen elicitors,
hormones,…)
THE1
MCA1 and FEI2
PEPR1/2
?
PROPEP1/3
Cell wall integrity
maintenance
Pattern-triggered
immunity
Stress responses
B
Cell wall damage
Other stimuli
(pathogen elicitors,
hormones,…)
THE1
MCA1 and FEI2
PEPR1/2
?
PROPEP1/3
Cell wall integrity
maintenance
Stress responses

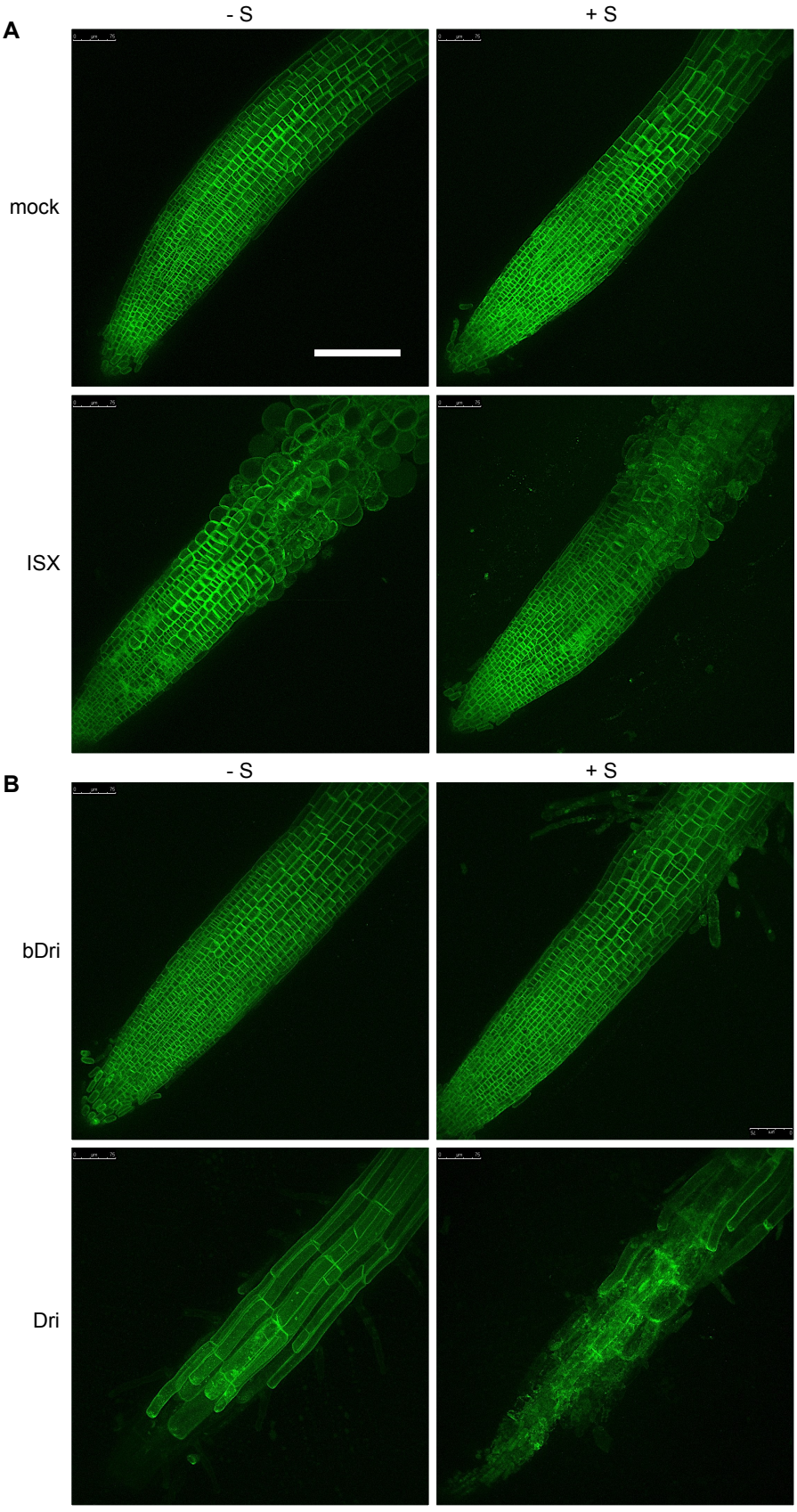

Fig. S1. Sorbitol modifies root responses to ISX and Driselase.
WAVE 131Y seedlings were treated with (**A**) DMSO (mock) or isoxaben (ISX) and (**B**) boiled Driselase (bDri) or Driselase (Dri) with or without sorbitol (+/-S). Root Z-stacks were taken after 7 h of treatment with confocal laser scanning microscope and 2D Images result from maximum intensity projection. (N = 3). Scale bar,150 µm.

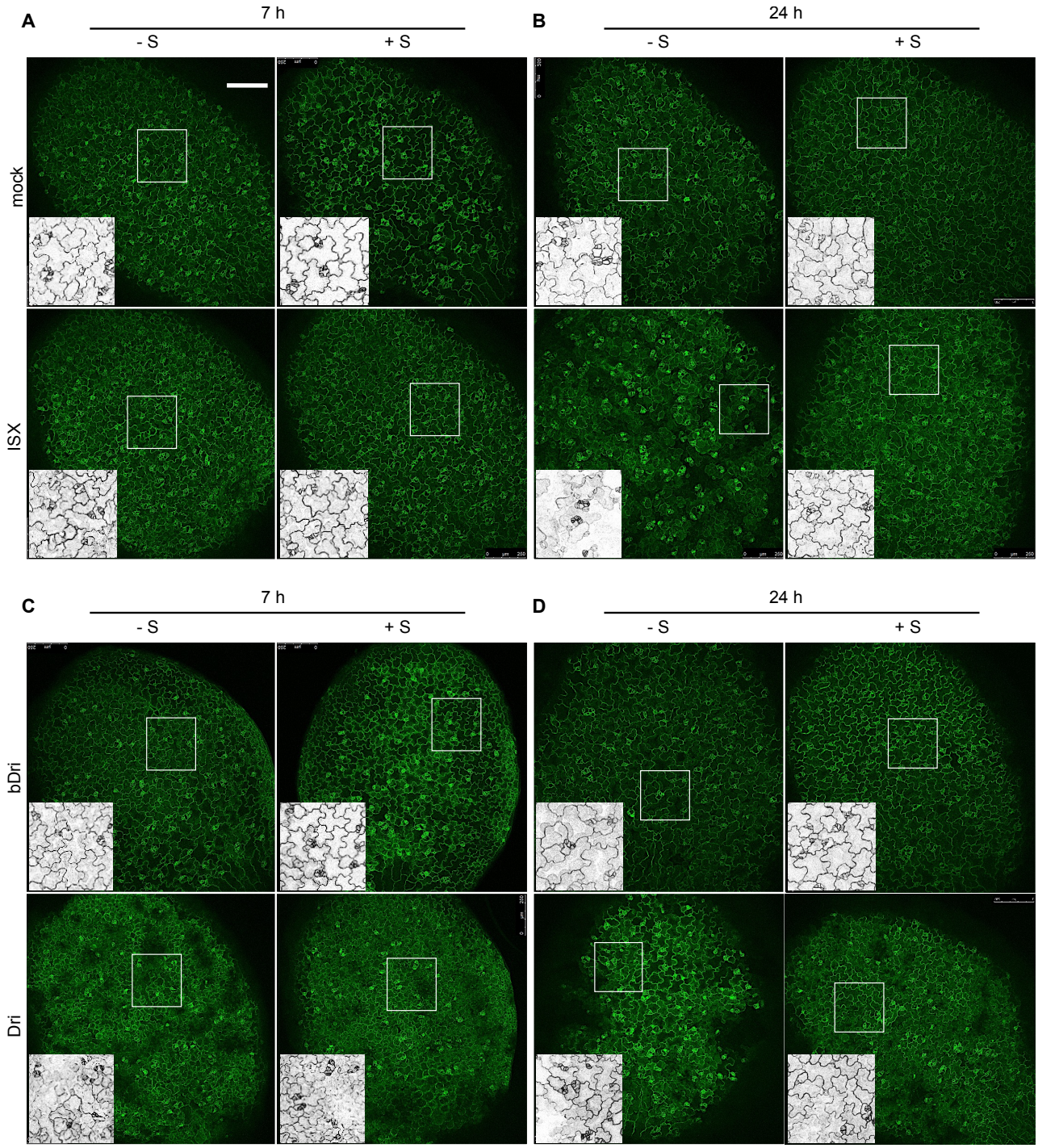

Fig. S2. Sorbitol modifies responses to ISX and Driselase in cotyledons.
WAVE 131Y seedlings were treated for (**A**) 7 h or (**B**) 24 h with DMSO (mock) or isoxaben (ISX) and for (**C**) 7 h or (**D**) 24 h with boiled Driselase (bDri) or Driselase (Dri) with or without sorbitol (+/-S). Z-stacks of cotyledons were taken with confocal laser scanning microscope and 2D Images result from maximum intensity projection (N = 3). Insets (highlighted by white rectangles on the Z-projection pictures) show cell outlines in selected areas. Scale bar, 250 µm.

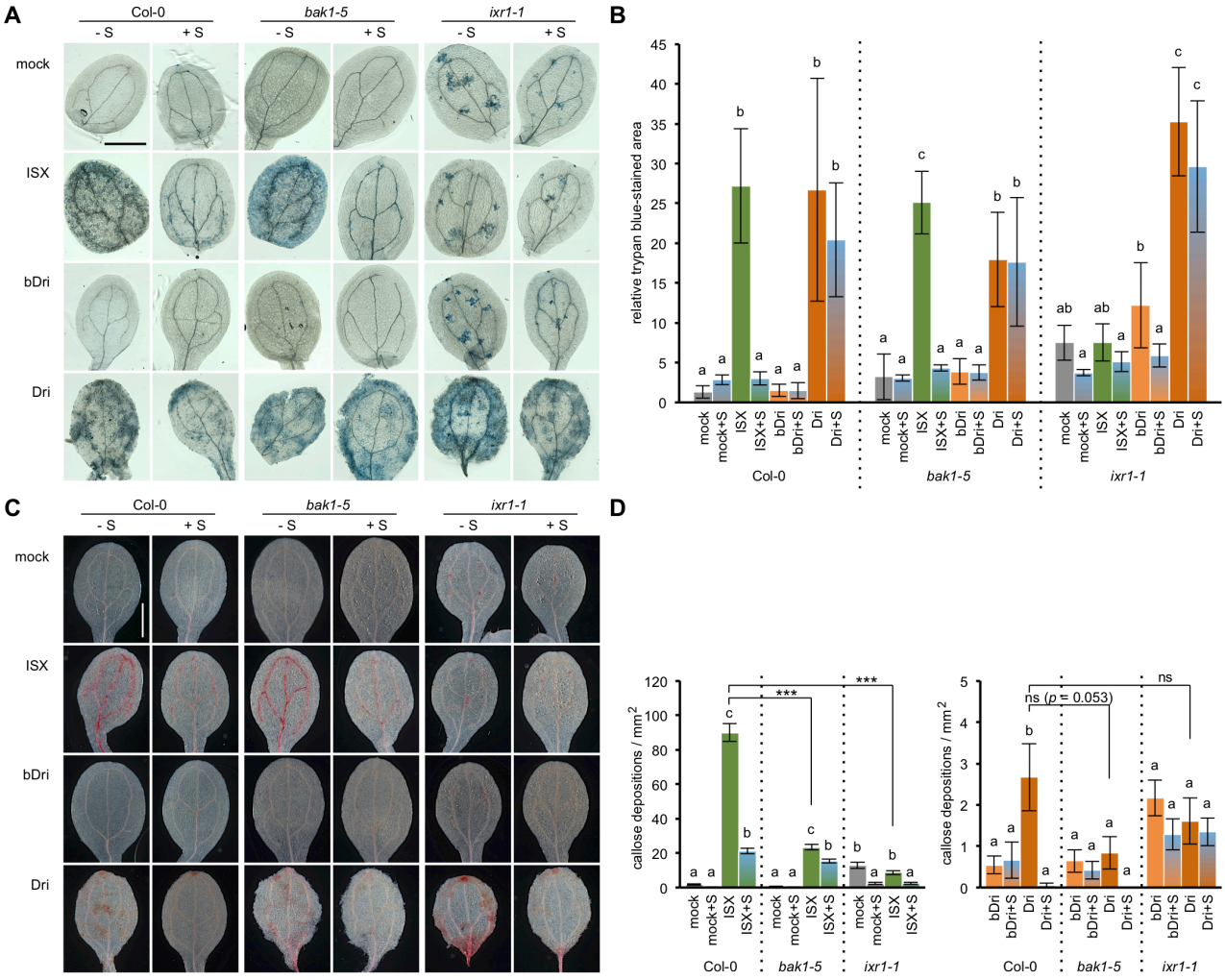

Fig. S3. CWD-induced cell death and lignin and callose production are sensitive to turgor manipulation.
Col-0, *bak1-5*, and *ixr1-1* seedlings were treated with DMSO (mock), isoxaben (ISX), boiled Driselase (bDri), or Driselase (Dri) with or without sorbitol (S). (**A**) Cell death in cotyledons was visualized 24 h after treatment by trypan blue staining. **(B)** Relative trypan blue-stained cotyledon areas were quantified with ImageJ. Values are means of individual cotyledons (N ≥ 8) ± SD. (**C**) Lignification in cotyledons was visualized by phloroglucinol staining (N ≥ 5). Scale bar, 1 mm. (**D**) Callose deposition in cotyledons was detected with Aniline blue. Values are means (N ≥ 15) ± SEM. Letters a–c (B, D) indicate statistically significant differences between treatments of each genotype according to one-way ANOVA and Tukey's HSD test (α = 0.05). Asterisks (D) indicate statistically significant differences compared to the wild-type (Student's *t*-test; *** $p < 0.001$; ns, not significant).

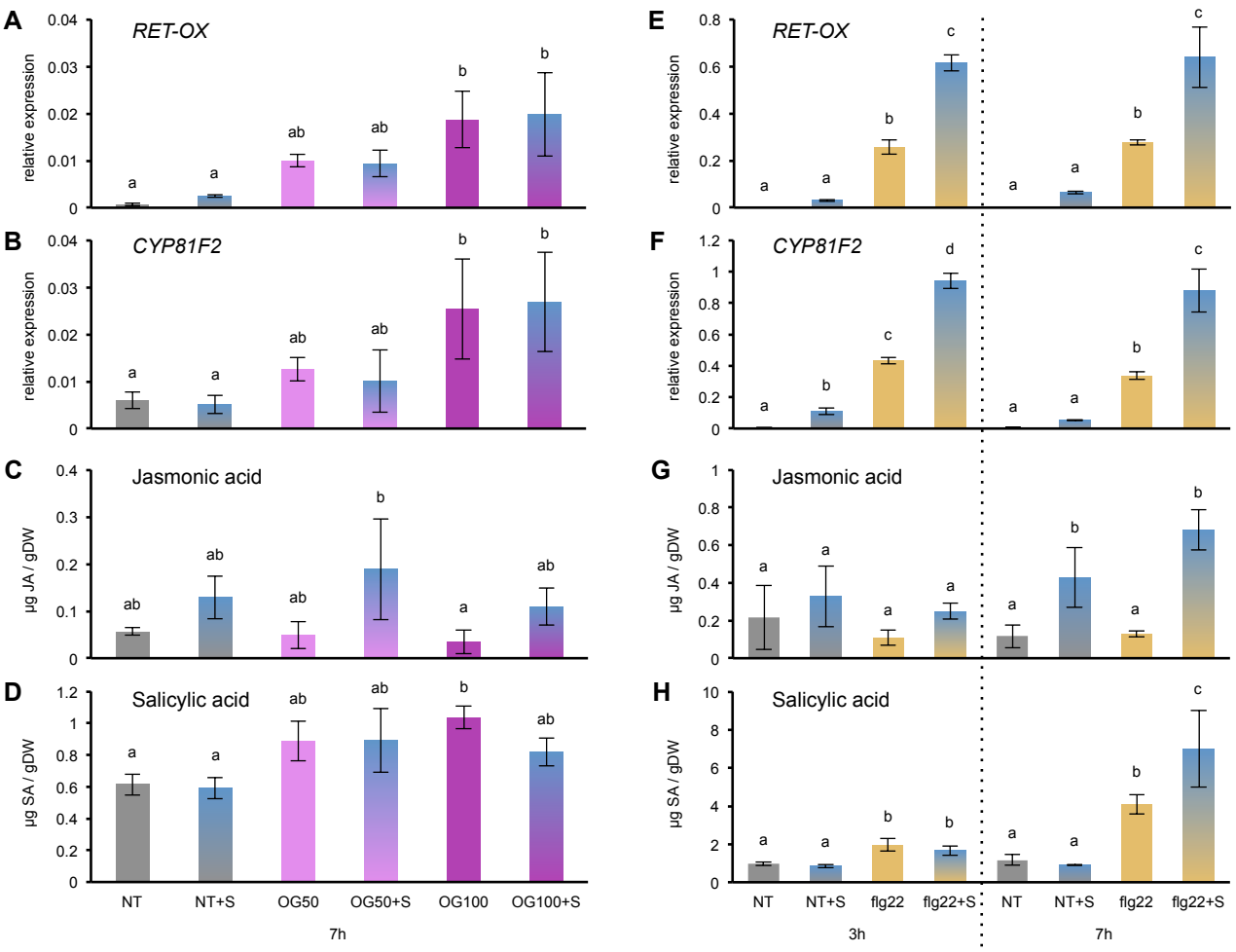

Fig. S4. Sorbitol does not reduce OG- and flg22-induced defense responses.
(A) Relative *RET-OX* and **(B)** *CYP81F2* expression quantified by qRT-PCR in Col-0 seedlings treated with 50 or 100 µg / ml oligogalacturonides (OG50, OG100), compared to untreated (NT) seedlings and co-treatments with sorbitol (S). **(C)** Amounts of JA and **(D)** SA in Col-0 seedlings treated as indicated. **(E)** Relative *RET-OX* expression, **(F)** relative *CYP81F2* expression, and production of **(G)** JA and **(H)** SA in Col-0 seedlings treated with mock conditions (NT), sorbitol (NT + S), 10 nM flg22 (flg 22), or 10 nM flg22 and sorbitol (flg22 + S). All values represent means (N = 3) with error bars indicating SD. Letters a–c indicate statistically significant differences according to one-way ANOVA and Tukey's HSD test ($\alpha = 0.05$) between treatments at each time point.

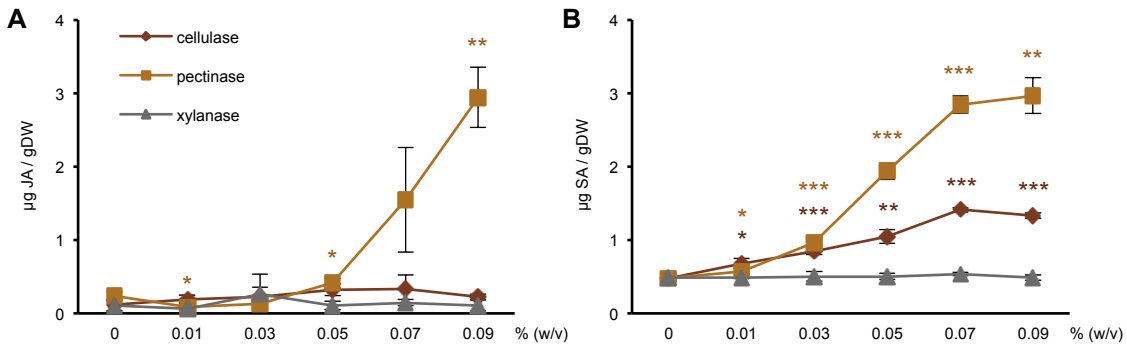

Fig. S5. Individual cell wall–degrading enzymes have specific effects on JA and SA accumulation.

(**A**) Jasmonic acid (JA) and (**B**) salicylic acid (SA) amounts were quantified in Col-0 seedlings at 7 h after treatment with 0, 0.01, 0.03, 0.05, 0.07, and 0.09 % (w/v) cellulase, pectinase, or xylanase. Values represent means (N = 3) with error bars indicating SD. Asterisks indicate statistically significant differences to 0 % (w/v) enzyme treatment according to Student's *t*-test (* $p < 0.05$; ** $p < 0.01$; *** $p < 0.001$).

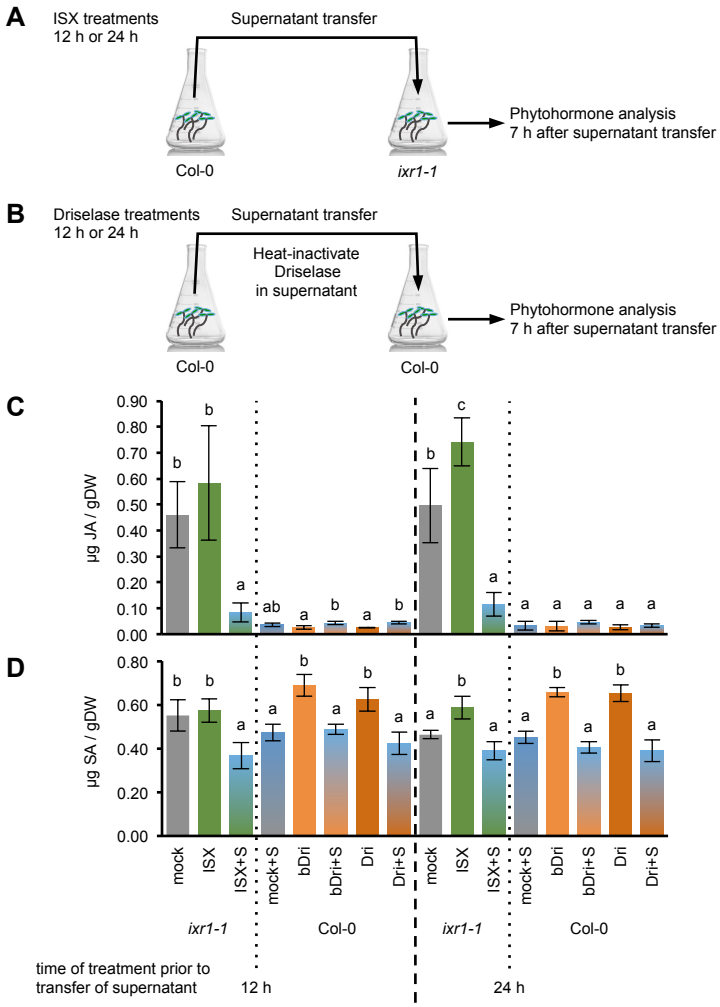

Fig. S6. Supernatants from damaged seedlings do not induce pronounced JA and SA accumulation.

(**A, B**) Schemes illustrating the experimental setup to investigate whether compounds secreted upon CWD elicit phytohormone accumulation. Col-0 seedlings were treated with DMSO (mock), Sorbitol (S), isoxaben (ISX), Driselase (Dri), boiled Dri (bDri), or combinations thereof for 12 or 24 h as indicated. Supernatants from mock, ISX, and ISX+S treatments were transferred onto *ixr1-1* seedlings (A) or boiled for 10 min and transferred on Col-0 seedlings (B). (**C**) Jasmonic acid (JA) and (**D**) Salicylic acid (SA) were quantified 7 h after the start of the incubation. Values are means (N = 4) with error bars indicating SD. Different letters between treatments of each genotype and time point indicate statistically significant differences according to one-way ANOVA and Tukey's HSD test ($\alpha = 0.05$).

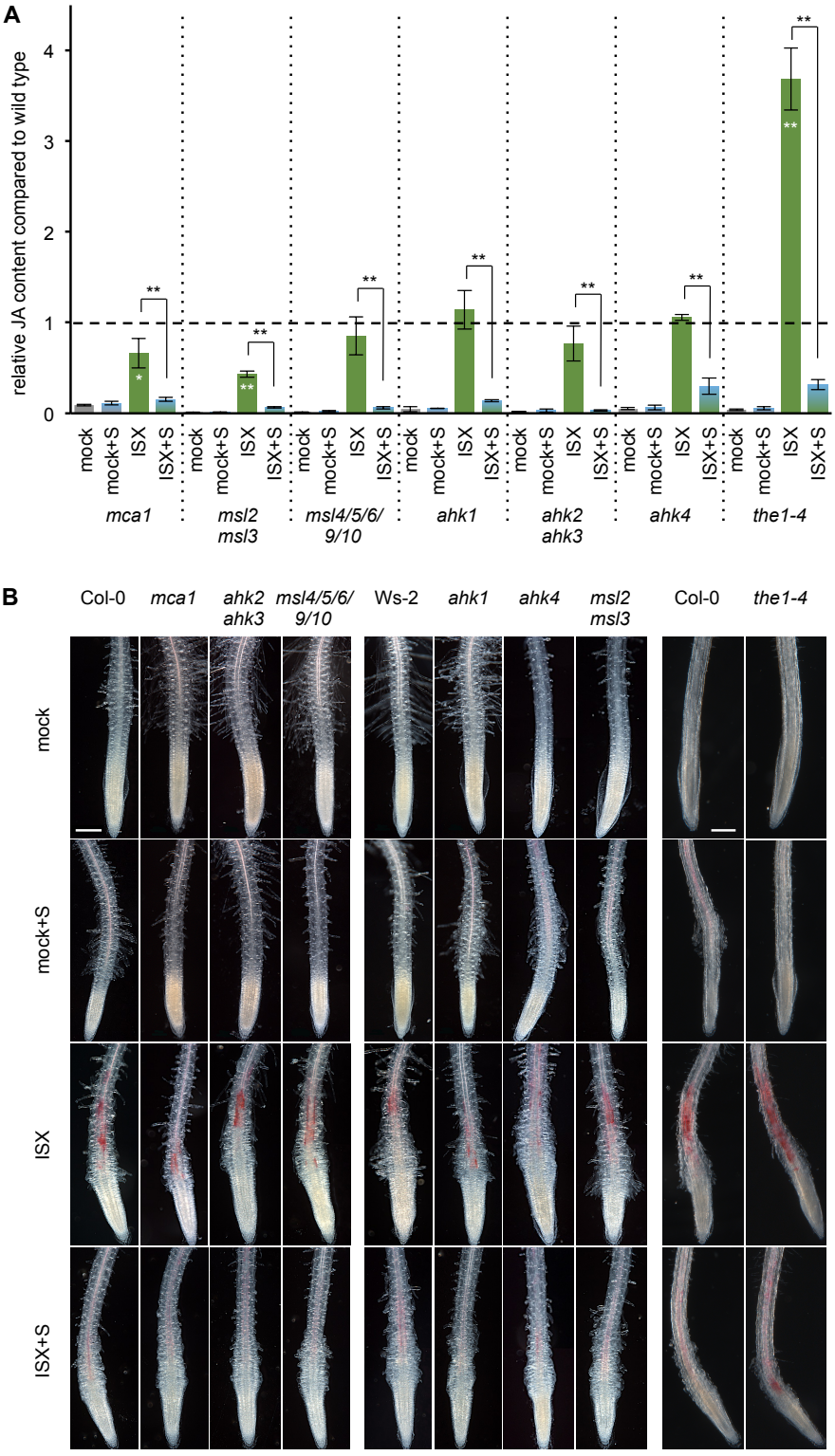

Fig. S7. ISX-induced CWD responses in osmosensing and mechanoperception mutants.
(**A**) Jasmonic acid (JA) accumulation was quantified in *mca1*, *msl2 msl3*, *msl4/5/6/9/10*, *ahk1*, *ahk2 ahk3, ahk4*, and *the1-4* seedlings after treatment with DMSO (mock), sorbitol (S), isoxaben (ISX) or combinations thereof. Values are relative to the respective ISX-treated wild type control (N ≥ 3, means ± SD). Asterisks indicate statistically significant differences to the wild type (white asterisks) or between treatments (black asterisks; Student's *t*-test, * $p < 0.05$, ** $p < 0.01$). (**B**) Col-0, *mca1*, *ahk2 ahk3*, *msl4/5/6/9/10*, Ws-2, *ahk1*, *ahk4, msl2 msl3*, and *the1-4* seedlings were stained with phloroglucinol after different treatments to visualize root tip lignification. N > 15. Scale bars, 200 µm.

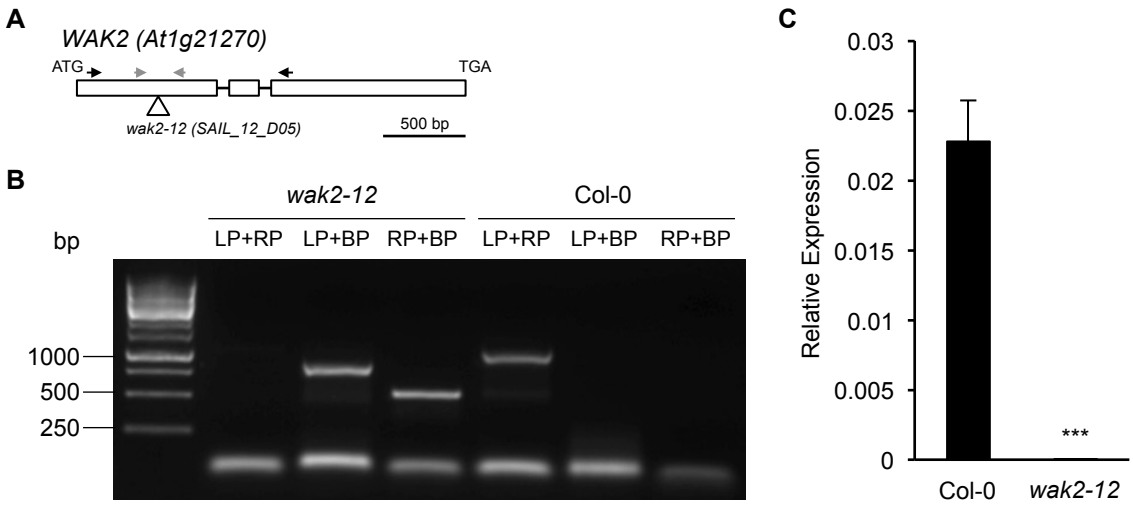

Fig. S8. Isolation of the *wak2-12* allele.
(**A**) Sketch of the *WAK2* gene. Boxes, exons; lines, introns; triangle, the SAIL_12_D05 T-DNA insertion site. Black arrows indicate primers used for the genotyping PCR reaction, whereas grey arrowheads indicate primers used for qRT-PCR analysis. (**B**) PCR-based genotyping analysis to confirm T-DNA insertion (N = 3). (**C**) *WAK2* expression relative to *ACT2* was determined by qRT-PCR in Col-0 and *wak2-12* seedlings. Values represent means (N = 3) with error bars indicating SD. Asterisks indicate a statistically significant difference (Student´s *t*-test; *** $p < 0.001$).

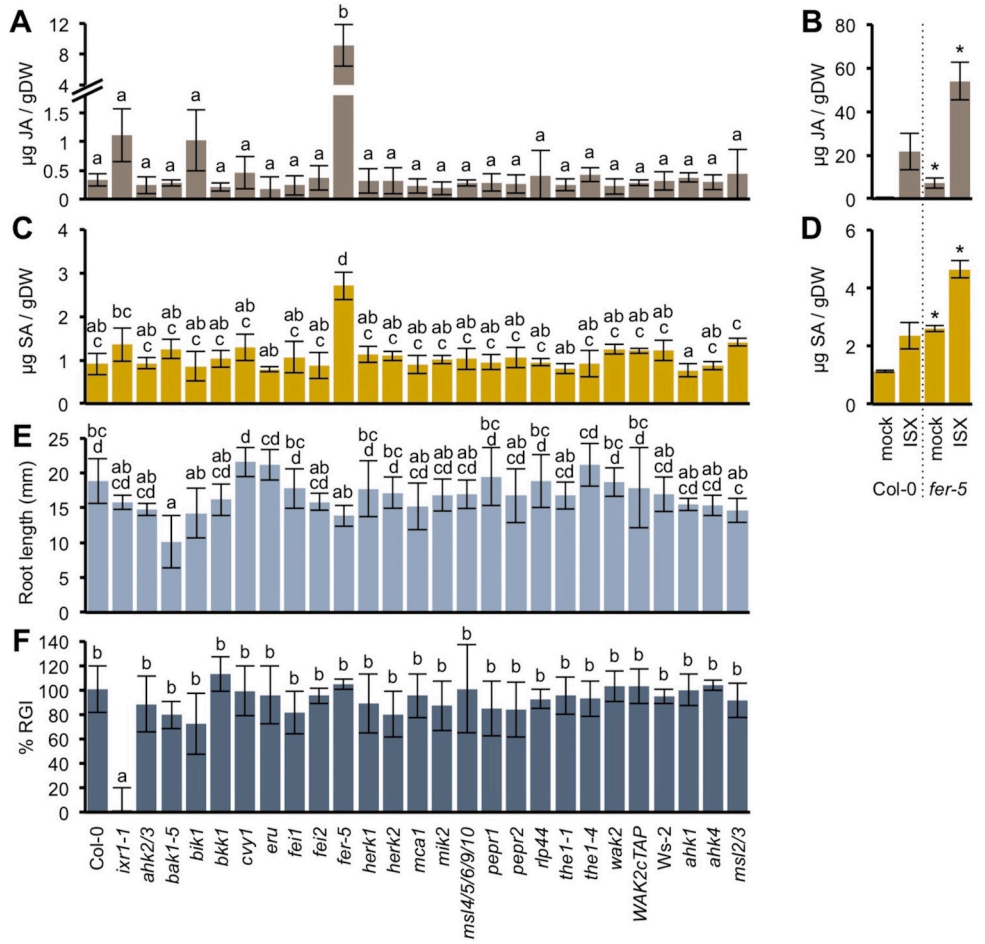

Fig. S9. JA and SA accumulation, root growth, and ISX resistance phenotypes in mock-treated mutant seedlings.

(**A**) JA amounts were quantified in the indicated mutant seedlings after DMSO (mock) treatment and in (**B**) Col-0 and *fer-5* seedlings after mock and isoxaben (ISX) treatment. SA amounts were quantified in (**C**) mutant seedlings after mock treatment and in (**D**) Col-0 and *fer-5* seedlings after mock and ISX treatment. (**E**) Root length and (**F**) ISX resistance (root growth inhibition, RGI) were determined in mutant seedlings. 100% indicates full sensitivity to ISX treatment, whereas 0% indicates complete resistance. Values in (A, C, E, F) represent the average of mean values from 3–8 independent experiments ± SD. Letters a–d indicate statistically significant differences according to one-way ANOVA and Tukey's HSD test ($\alpha = 0.05$) between genotypes. Values in (B, D) represent means (N = 3) with error bars indicating SD. Asterisks indicate statistically significant differences to the wild type (Student's *t*-test, * $p < 0.05$).

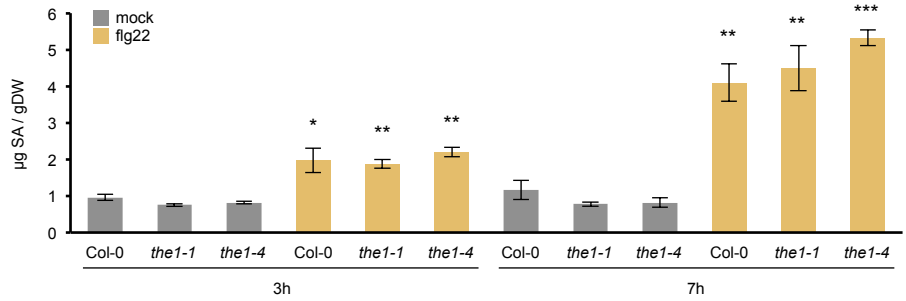

Fig. S10. THE1 is not required for flg22-induced SA accumulation.
SA quantification in Col-0, *the1-1*, and *the1-4* seedlings either mock-treated or with 10 nM flg22. Data belongs to the same data set as Figure S4H. Values represent means (N = 3) with error bars indicating SD. Asterisks indicate statistically significant differences to the respective mock control according to Student's *t*-test (* $p < 0.05$; ** $p < 0.01$; *** $p < 0.001$).

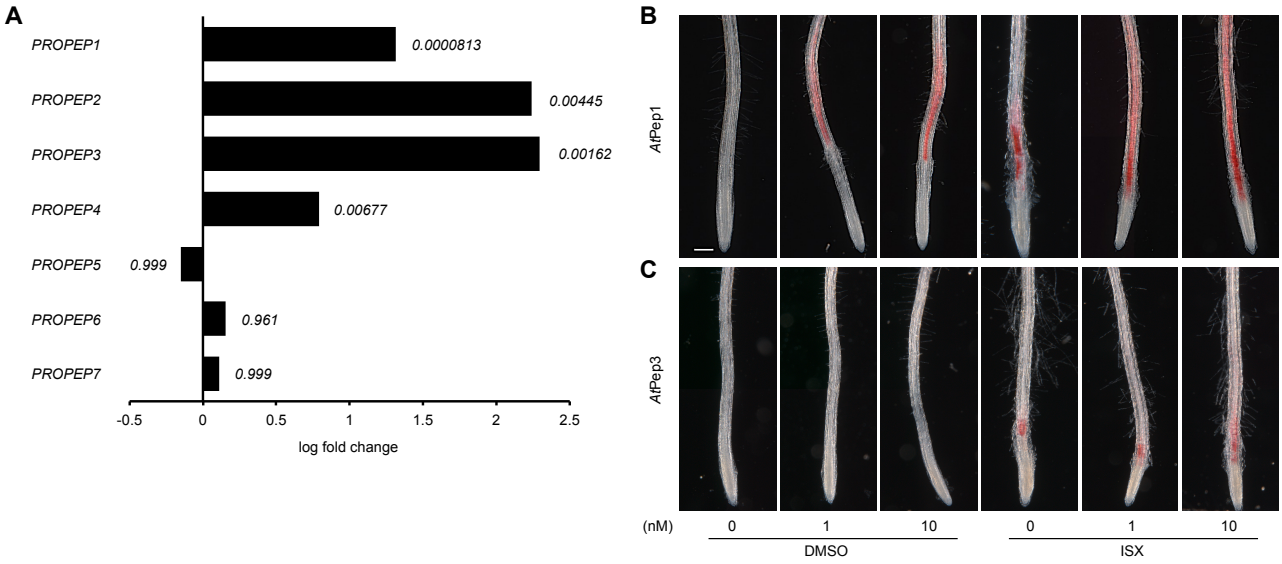

Fig. S11. *PROPEP1-7* expression in ISX-treated seedlings and effects of *At*Pep1 and *At*Pep3 treatments on lignin production.

(**A**) Col-0 seedlings were treated with DMSO (mock) or isoxaben (ISX). Changes in gene expression were analyzed after 1 h using RNA-Seq (see Supplemental File S1). ISX-induced changes in the expression of *PROPEP1, PROPEP2, PROPEP3, PROPEP4, PROPEP5, PROPEP6*, and *PROPEP7* are plotted on a $\log_2$ scale, and *p*-values are given next to the individual bars (N = 3). (**B, C**) Root tip lignification in Col-0 seedlings was visualized by phloroglucinol staining (N ≥ 6) after mock treatment (DMSO, 0), ISX treatment (ISX, 0), or co-treatments with 1 and 10 nM *At*Pep1 (B) or 1 and 10 nM *At*Pep3 (C). Scale bar, 200 µm.

Table S1. GO enrichment analysis of genes with ISX-dependent expression changes.
Genes with significantly altered expression after 1 h of ISX-treatment (Supplemental File S1) have been analyzed for GO enrichment using the PANTHER Overrepresentation Test (release 20160715) and the GO Ontology database (Released 2017-02-28) on http://geneontology.org/. Results are filtered by $P < 0.05$ after Bonferroni correction for multiple testing.

GO biological process complete	*Arabidopsis thaliana* - REFLIST (27352)	ISX-dependent (109)	Expected	Over/under	fold enrichment	P-value
salicylic acid mediated signaling pathway (GO:0009863)	38	5	.15	+	32.72	1.19E-03
response to hypoxia (GO:0001666)	52	5	.21	+	23.91	5.45E-03
response to chitin (GO:0010200)	109	10	.44	+	22.81	6.97E-08
cellular response to salicylic acid stimulus (GO:0071446)	55	5	.22	+	22.60	7.14E-03
response to decreased oxygen levels (GO:0036293)	59	5	.24	+	21.07	1.00E-02
response to oxygen levels (GO:0070482)	60	5	.24	+	20.72	1.09E-02
response to organonitrogen compound (GO:0010243)	136	10	.55	+	18.28	5.83E-07
response to nitrogen compound (GO:1901698)	210	10	.84	+	11.84	3.51E-05
response to salicylic acid (GO:0009751)	170	8	.68	+	11.70	1.10E-03
response to jasmonic acid (GO:0009753)	177	7	.71	+	9.83	1.79E-02
response to wounding (GO:0009611)	185	7	.74	+	9.41	2.37E-02
innate immune response (GO:0045087)	239	8	.96	+	8.32	1.33E-02
immune response (GO:0006955)	244	8	.98	+	8.15	1.55E-02
response to organic cyclic compound (GO:0014070)	284	9	1.14	+	7.88	5.36E-03
response to oxidative stress (GO:0006979)	354	11	1.42	+	7.73	4.75E-04
immune system process (GO:0002376)	275	8	1.11	+	7.23	3.64E-02
defense response to bacterium (GO:0042742)	278	8	1.12	+	7.16	3.93E-02
response to bacterium (GO:0009617)	350	10	1.41	+	7.10	3.65E-03
response to oxygen-containing compound (GO:1901700)	1159	23	4.66	+	4.93	4.49E-07
defense response (GO:0006952)	1267	24	5.10	+	4.71	4.32E-07
response to endogenous stimulus (GO:0009719)	1293	23	5.20	+	4.42	3.64E-06
response to acid chemical (GO:0001101)	904	16	3.64	+	4.40	1.56E-03
response to organic substance (GO:0010033)	1482	25	5.96	+	4.19	1.84E-06
response to other organism (GO:0051707)	995	15	4.00	+	3.75	2.44E-02
response to external biotic stimulus (GO:0043207)	997	15	4.01	+	3.74	2.50E-02
response to chemical (GO:0042221)	2075	30	8.34	+	3.60	1.02E-06
response to biotic stimulus (GO:0009607)	1038	15	4.17	+	3.59	3.99E-02
response to hormone (GO:0009725)	1210	17	4.87	+	3.49	1.51E-02
signal transduction (GO:0007165)	1484	20	5.97	+	3.35	3.95E-03
single organism signaling (GO:0044700)	1512	20	6.08	+	3.29	5.24E-03
signaling (GO:0023052)	1513	20	6.08	+	3.29	5.30E-03
multi-organism process (GO:0051704)	1320	17	5.31	+	3.20	4.61E-02
response to stress (GO:0006950)	2696	34	10.84	+	3.14	1.81E-06
cellular response to stimulus (GO:0051716)	2115	26	8.51	+	3.06	4.89E-04
cell communication (GO:0007154)	1662	20	6.68	+	2.99	2.13E-02
response to stimulus (GO:0050896)	4701	45	18.91	+	2.38	8.72E-06
regulation of cellular process (GO:0050794)	3722	34	14.97	+	2.27	4.77E-03
regulation of biological process (GO:0050789)	4061	34	16.33	+	2.08	3.25E-02
Unclassified (UNCLASSIFIED)	7940	30	31.93	-	.94	0.00E00

Table S2. *Arabidopsis* genotypes used in this study. Names used in this work are listed along with gene identifiers, specific allele used, genetic background, and references.

Gene(s)	AGI	Allele	Background	Reference
AHK1	*At2g17820*	*ahk1-3*	Ws-2	(78)
AHK2 AHK3	*At5g35750, At1g27320*	*ahk2-2 ahk3-3*	Col-0	(79)
AHK4	*At2g01830*	*cre1-10*	Ws-2	(79)
BAK1	*At4g33430*	*bak1-5*	Col-0	(53)
BIK1	*At2g39660*	*bik1*	Col-0	(80)
BKK1	*At2g13790*	*bkk1-1*	Col-0	(53)
CVY1	*At2g39360*	*cvy1*	Col-0	(81)
ERU	*At5g61350*	*eru-2*	Col-0	(82, 83)
FEI1	*At1g31420*	*fei1*	Col-0	(84)
FEI2	*At2g35620*	*fei2-2*	Col-0	(84)
FER	*At3g51550*	*fer-5*	Col-0	(85)
HERK1	*At3g46290*	*herk1*	Col-0	(86)
HERK2	*At1g30570*	*herk2*	Col-0	(86)
IXR1	*At5g05170*	*ixr1-1*	Col-0	(52)
MCA1	*At4g35920*	*mca1-null*	Col-0	(20)
MIK2	*At4g08850*	*mik2-1*	Col-0	(24)
MSL2 MSL3	*At5g10490, At1g58200*	*msl2-1 msl3-1*	Ws-2	(87)
MSL4/5/6/9/10	*At1g53470, At3g14810, At1g78610, At5g19520, At5g12080*	*msl4-1 msl5-2 msl6-1 msl9-1 msl10-1*	Col-0	(88)
PEPR1	*At1g73080*	*pepr1-2*	Col-0	(89)
PEPR2	*At1g17750*	*pepr2-1*	Col-0	(89)
PEPR1 PEPR2	*At1g73080, At1g17750*	*pepr1-1 pepr2-1*	Col-0	(89)
RLP44	*At3g49750*	*rlp44-3*	Col-0	(62)
THE1	*At5g54380*	*the1-1*	Col-0	(21)
THE1	*At5g54380*	*the1-4*	Col-0	(86)
WAK2	*At1g21270*	*SAIL_12_D05 (wak2-12)*	Col-0	
WAK2cTAP	*At1g21270*	*35S:WAK2cTAP*	Col-0	(23)
pPROPEP3::PROPEP3-VENUS	*At5g64905*		Col-0	(67)

Table S3. Primers used in this study.

GENE	AGI CODE	LP	RP		Ref
TCH4	At5g57560	GATCACTTGGGGTGATGGTC	GGGACAAGCTTCATTTGCAT	qRT-PCR	(12)
PDF1.2	At5g44420	CGCACCGGCAATGGTGG	ATCCATGTTTGGCTCCTTCG	qRT-PCR	(57)
RET-OX	At1g26380	AGGTTCTCGAACCCTAACAACA	GCACAGACGACACGTAAGAAAG	qRT-PCR	(57)
CYP81F2	At5g57220	GTGAAAGCACTAGGCGAAGC	ATCCGTTCCAGCTAGCATCA	qRT-PCR	(57)
WAK2	At1g21270	CGCACATCTGGAGTTGAAAA	GAGAAAGGCGTAGGTGCAAG	qRT-PCR	
PROPEP1	At5g64900	GAAATCAGATAGACGAAGCGAA	CCATGGTAACGTCTTCTTTTT	qRT-PCR	
PROPEP2	At5g64890	TCACCAAACTATTGGATTTCAA	GACTCAATTTTTGACTTCTTAATCC	qRT-PCR	
PROPEP3	At5g64905	CAACGATGGAGAATCTCAGA	CTAATTGTGTTTGCCTCCTTT	qRT-PCR	
PROPEP4	At5g09980	AACTTAGCTCTCACGAAGCA	AAAAATAAAGGACTCGTAGGAGTT	qRT-PCR	
PP2A	At1g13320	TAACGTGGCCAAAATGATGC	GTTCTCCACAACCGCTTGGT	qRT-PCR	(90)
ACT2	At3g18780	CTTGCACCAAGCAGCATGAA	CCGATCCAGACACTGTACTTCCTT	qRT-PCR	(90)
UBA1	At2g30110	TGAGTGCTGGTGATGCTCAG	TCCTCAAACCTCAGTCGTGC	qRT-PCR	
GRF2	At1g78300	TCGTCTTGGTCTTGCATTGAA	ATCAAAGGCCTGTTTGGCGA	qRT-PCR	
WAK2	At1g21270	CAAGCATGATAACCGAGAAGC	CCCTTTTGGTACTTCTCCAGG	genotyping PCR	
SAIL LB1	GCCTTTTCAGAAATGGATAAATAGCCTTGCTTCC			genotyping PCR	(91)

Data file S1. Transcriptomics data.
The transcriptomics data, including the candidate genes we identified, are provided in a separate Excel file. Col-0 and *ixr1-1* seedlings were treated with DMSO or ISX and analyzed by RNA-Seq 1 h after treatment. Raw data from three independent biological replicates are shown in the "raw data" tab. 109 transcripts found differentially regulated after ISX- compared to DMSO- treatment ($p < 0.01$) are shown in the tab "Col ISX vs DMSO". Up- or downregulated transcripts compared to DMSO controls are color- coded orange (up) or blue (down). Fold changes of *PROPEP1, PROPEP 2, PROPEP 3, PROPEP 4, PROPEP 5, PROPEP 6* and *PROPEP 7* transcripts are calculated in tab "PROPEP ISX vs DMSO" and plotted in Supplemental Fig. S11 A. In tab "*ixr1-1* vs. Col-0 DMSO" 2317 transcripts are found to be differentially expressed between mock-treated Col-0 and *ixr1-1* seedlings.

Data file S2. Peptide mass fingerprinting data.
The proteomics data are provided in a separate Excel file.